

ASSESSMENT OF HEMODYNAMIC PARAMETERS USING 4D FLOW MRI

MATTIAS ANDERSSON

Master's thesis
2018:E34



LUND UNIVERSITY

Faculty of Engineering
Centre for Mathematical Sciences
Mathematics

LTH

Assessment of hemodynamic parameters using 4D Flow MRI

Mattias Andersson

Author:

Mattias Andersson - tfy13man@student.lu.se, 0736-835533

Supervisors:

Niels Christian Overgaard - nco@maths.lth.se

Mariana Bustamante - mariana.bustamante@liu.se

Examiner:

Kalle Åström - karl.astrom@math.lth.se

Preliminary dates:

Start: 22-01-2018

End: 12-06-2018

28-05-2018

Abstract (English)

Heart disease is one of the worldwide leading causes of death, and facilitating the work of physicians in this area is therefore of great importance. Imaging of the heart is one of many fields that is used for diagnosis and analysis of cardiac disease. Within this field, Magnetic Resonance Imaging (MRI) is a non-invasive technique that allows for acquisition of high quality images.

Blood flow throughout the healthy human body seems to follow certain patterns. Changes in the blood flow behaviour through the heart can be observed in the presence of cardiac disease. For the cardiac system, blood flow and parameters related to blood flow are important markers for such disease. This thesis aims to create a tool that uses blood flow data obtained from four-dimensional Flow MRI (4D Flow MRI) to calculate and assess hemodynamic (blood flow related) parameters that reflect such alterations in blood flow.

This hemodynamic assessment tool allows for easy visualisation and comparison of parameters in different regions of the heart, including the four cardiac chambers, aorta and pulmonary artery. Furthermore, the output of the tool allows for statistical analysis of hemodynamic parameters.

The tool was applied to a cohort of 4D Flow data sets. Examples of parameter visualisations are provided, and a statistical analysis of the parameters with regards to left ventricular ejection fraction was performed. This analysis was performed using self-organising feature maps, but did not show any significant results. This may be due to the heterogeneity of the data however, and not due to the tool in itself.

Abstract (Svenska)

Hjärtsjukdomar är en av de vanligaste dödsorsakerna i världen, och att underlätta arbetet för läkare inom detta område är därför av stor vikt. Avbildning av hjärtat är ett av många sätt som används som stöd för diagnostisering och analys av dessa sjukdomar. Inom detta område är magnetisk resonanstomografi (MRT) en icke-invasiv metod som möjliggör framtagning av bilder av hög kvalitet.

Blodflödet genom den friska kroppen verkar följa vissa mönster, men vid kardiovaskulära sjukdomar kan fluktuationer i flödet genom hjärtat observeras. I det kardiovaskulära systemet är blodflödet och parametrar relaterade till blodflöde viktiga markörer för sjukdom. Denna avhandling har som syfte att skapa ett verktyg som använder flödesdata från fyrdimensionell flödes MRT (4D flödes-MRT) för att räkna ut hemodynamiska (blodflödesrelaterade) parametrar som reflekterar sådana fluktuationer i blodflöde.

Verktyget möjliggör lättillgänglig visualisering och jämförelse av parametrar i olika områden i hjärtat. Bland dessa finns hjärtats fyra rum, aorta samt lungartären. Resultaten från verktyget kan även med fördel användas för statistisk analys av hemodynamiska parametrar.

Med verktyget i hand applicerades det på en kohort av 4D flödes dataset. Exempel på visualisering av parametrar tillhandahålls, och en statistisk analys av parameterarna med avseende på ejektionsfraktion i vänster kammare utfördes. Denna analys utfördes med hjälp av self-organising feature maps, men gav inga signifikanta resultat.

Preface

Before you lies the master thesis report “Analysis of hemodynamic parameters using 4D Flow MRI“. The basis of this thesis is the development of a tool that calculates and visualises hemodynamic parameters. The thesis has been written to fulfill the graduation requirements of the Engineering Physics MSc program at Lunds tekniska högskola (LTH), a part of Lund University. I was working with this thesis from January to June 2018.

The project was undertaken at the Linköping cardiovascular magnetic resonance (CMR) group. My main supervisors for this project have been Mariana Bustamante, in Linköping, and Niels Christian Overgaard, in Lund.

Acknowledgements

I would like to thank my supervisor, Mariana Bustamante, for the immense amount of help and encouragement she has provided me with over the course of this project. I would also like to thank the head of the CMR department, Tino Ebbers, as well as Petter Dyverfeldt for giving me the opportunity to do my master thesis work here. Thanks are also due to Niels Christian Overgaard for his assistance when it comes to the writing of this report. Furthermore, thanks are in order for the entire crew of the CMR department, employees and other master students alike. The talks, laughters, lunch adventures and fika moments have added to the enjoyment of performing this project.

Last, but not least, I would like to thank the people close to me. First Eva, for making me move here, for all the love and all the support. I also want to thank my mother for always believing in and caring about me. A big thank you to my father, whose belief in me never was as clearly expressed as that of my mother, but who nevertheless always provided encouragement. Without the thirst for knowledge that you have imprinted on me, I would not have ended up where I am today.

Contents

1	Introduction	1
1.1	Aims	1
2	Background	1
2.1	The human heart	1
2.1.1	Cardiac anatomy	2
2.1.2	Blood flow through the heart	3
2.1.3	Ejection fraction	3
2.2	4D Flow MRI	4
2.3	Atlas based segmentation	4
3	Theory	5
3.1	Hemodynamic parameters	5
3.1.1	Speed	6
3.1.2	Kinetic energy	6
3.1.3	Turbulent kinetic energy	7
3.1.4	Helicity	8
3.1.5	E-A wave related parameters	9
3.1.6	Pressure	9
3.2	Data analysis techniques	10
3.2.1	Self-organizing map	11
3.2.2	Bayes' theorem	11
3.2.3	Feature scaling	11

4	Methods	12
4.1	Study population	12
4.2	Acquisition settings	12
4.3	Implementation details	13
4.3.1	Finding systole/diastole	13
4.3.2	Pressure difference	14
4.3.3	Obtaining and visualising results	15
4.4	Post-processing of results	16
4.4.1	Comparison between data sets	16
4.4.2	Data analysis	20
5	Results	21
5.1	Parameter visualisations	21
5.1.1	A single data set	21
5.1.2	Volume renderings	28
5.1.3	Average curves - example	30
5.1.4	Comparison between a patient and average healthy data sets	31
5.2	SOFM Clustering	33
5.3	Posterior probabilities	35
6	Discussion	36
6.1	The results	36
6.1.1	Parameter visualisation	36
6.1.2	Data analysis	37
6.2	The hemodynamic assessment tool	39

6.3 Future work	40
7 Conclusions	41
8 References	42

1 Introduction

Blood flow throughout the healthy human body seems to follow certain patterns [1]. In the presence of cardiac disease, changes in the blood flow behaviour through the heart can be observed. Such changes are seen early on in the development of the disease, which makes the analysis of blood flow a potentially powerful tool when it comes to early treatment of cardiac disease, as these alterations in flow have turned out to be quite difficult to predict based on anatomy alone [2]. Blood flow velocity can be measured in the whole heart using four-dimensional Flow Magnetic Resonance Imaging (4D Flow MRI) [3], but manual analysis of this data has been shown to be extremely difficult and time-consuming. With this challenge in mind, a technique to automatically segment the cardiac chambers and major thoracic vessels in 4D Flow MR images has been developed by the cardiovascular MR (CMR) group at Linköping University. The proposed method results in segmentations suitable for the assessment of hemodynamic markers such as kinetic energy, pressure, helicity, vorticity, flow connectivity, among others [4], in a cohort of 4D Flow MRI datasets. These hemodynamic parameters could indicate altered blood flow patterns in the heart and major cardiac vessels, and thus be used as an early warning sign for cardiac disease [5, 6, 7].

1.1 Aims

The main goal of this project is to derive and analyse a number of hemodynamic parameters from 4D Flow MRI data in a cohort of patients. The included parameters were chosen through study of literature and articles related to the field, and their calculation will be implemented in an easy to use tool. Furthermore, an extended aim is also to attempt to answer the question of whether a correlation between these parameter values and cardiac disease can be found. This question will be answered by calculating a group of hemodynamic parameters for a data set consisting of 4D blood flow data from patients with different degrees of cardiac illness as well as from healthy volunteers. The presence of correlation will be evaluated by performing a statistical analysis of the hemodynamic parameters with regards to the illness of the patient.

2 Background

2.1 The human heart

The information presented in this section is largely based on Chapter 11 in the book “The Mechanics of the Circulation” [8].

2.1.1 Cardiac anatomy

The human heart can be described as the pump that enables blood circulation in the body. The heart consists of four different chambers — the left and right atria and ventricles. These, along with the other anatomical structures referred to in this section can be seen in fig.1. The atria are low-pressure chambers where blood comes in from the body. From there the blood passes on into the corresponding ventricles, which are high-pressure chambers. From the ventricles, the blood is then pumped out to the body through a major thoracic blood vessel — the aorta for the left side and the pulmonary artery for the right. Low-oxygen blood comes into the right hand side, and is pumped to the lungs. It is then passed on to the left hand side of the heart, and from there it is pumped out to the rest of the body.

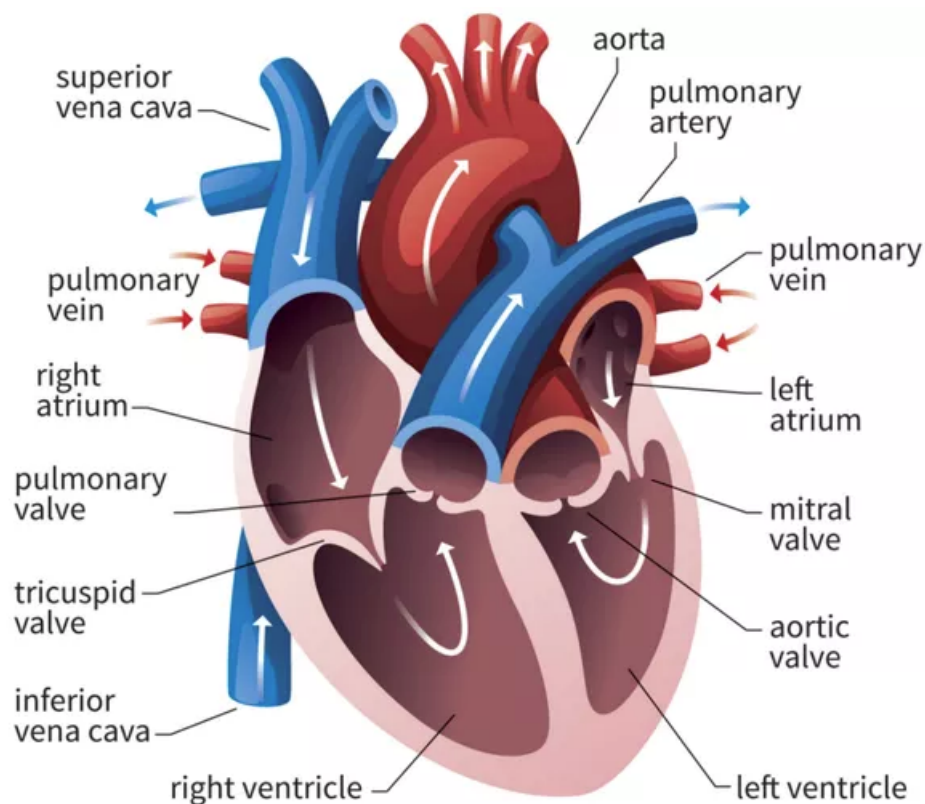


Figure 1: Cross section of a human heart [9]

These six anatomical regions — the left atrium and ventricle, the right atrium and ventricle, the aorta and the pulmonary artery are the regions of focus for this project. Other anatomical structures of interest are the valves that exist between the cardiac chambers (the atrio-ventricular valves) as well as between the ventricles and the two blood vessels of interest. These valves open and close to enable forward flow and prevent blood regurgitation. Between the right atrium and ventricle lies the tricuspid valve. The corresponding valve on the left side of the heart is called the mitral valve. The valves between the ventricles and out-flow blood

vessels are called the pulmonary and aortic valves.

2.1.2 Blood flow through the heart

The process where blood enters the atria, flows through to the ventricles and gets pumped out through the aorta and pulmonary artery is called a *cardiac cycle*. The cardiac cycle consists of two main phases: *systole* and *diastole*. These two phases occur cyclically. For the duration of this report and project, systole will be said to occur before diastole (so that one cardiac cycle is systole-diastole). Blood resides in the ventricles of the heart at the start of systole, and the mitral and tricuspid valves, as well as the aortic and pulmonary valves are closed. At this stage, pressure is building up in the ventricles, and when the ventricular pressure exceeds that of the aorta and pulmonary artery, the corresponding valves are opened, and blood flows through. As blood leaves the ventricles, the pressure difference between the ventricles and the arteries is reversed and the valves close. This marks the end of systole and the beginning of diastole. As the ventricle relaxes, blood flows into the atria, causing the pressure there to rise. When the pressure difference between the atria and the ventricles is large enough, the mitral and tricuspid valves open, and blood flows into the ventricles. This causes the pressure difference to reverse, which closes the atrio-ventricular valves, and the cardiac cycle is complete. Normally, systole constitutes about one third of the heart cycle, and diastole about two thirds.

Understanding of these two phases — systole and diastole — and what events in the cardiac cycle they correspond to, is important for the assessment and interpretation of many of the calculations and results in this report.

2.1.3 Ejection fraction

Ejection fraction is a parameter describing how much of the blood is ejected from a cardiac chamber with each stroke of the heart. Commonly the left ventricular ejection fraction (LVEF, from here on referred to simply as EF) is used as one of several measures of the blood pumping efficiency of the heart. It is used to manage and assess various cardiovascular diseases [10].

The EF is calculated as the volume of pumped blood divided by the total blood volume in the ventricle. One way to assess this is to use volume measurements of the left ventricle at end systole (ESV), when blood has been pumped through to the aorta, and end diastole (EDV), when the ventricle has been filled. EF can then be calculated as

$$EF = \frac{EDV - ESV}{EDV} \quad (1)$$

There is discussion among experts regarding the lower limit of EF that can be considered healthy. Cases have been presented which supports the notion that an EF above 50% is

considered normal [11], whereas other studies have shown other numbers, such as 57% [12].

2.2 4D Flow MRI

Four-dimensional flow magnetic resonance imaging (4D Flow MRI) is a technique used to enable analysis of blood flow throughout the body, for example in the heart and the major thoracic vessels. It is based on phase-contrast magnetic resonance imaging (PC MRI), which has been used for quantification and analysis of blood flow. In a 4D flow consensus document published in 2015, the authors Dyverfeldt et al. [13] stated that “*‘4D Flow CMR’ refers to phase-contrast CMR with flow-encoding in all three spatial directions that is resolved relative to all three dimensions of space and to the dimension of time along the cardiac cycle (3D + time = 4D)*”. In other words, flow data from 4D Flow MRI is obtained as blood velocities in three dimensions, over time (often one cardiac cycle).

The data this project is based on is velocity data obtained using the 4D Flow MRI acquisition technique. As the technique itself is not used, it will not be explained further here. Instead, the interested reader is directed to the consensus document by Dyverfeldt et al mentioned above.

2.3 Atlas based segmentation

In general terms, segmentation is the process of dividing a large set of data into smaller pieces. In the field of computer vision, segmentation is a commonly used tool. Segmentation of an image, or volume, means dividing the image into several different segments of interest, by assigning a semantic label to each pixel or voxel. How these segments are chosen depends entirely of what interest one has in the image or volume. When it comes to 4D flow analysis of the heart, natural regions of interest are the four cardiac chambers, as well as two of the major thoracic blood vessels — the aorta and the pulmonary artery. There are several different approaches to segmentation, with various methods having different uses for different purposes.

One method of segmentation is atlas based segmentation. The information conveyed on this subject in this report is largely based on the report *Quo vadis, Atlas-based segmentation?* by Rohlfing et al. [14], and for further understanding of this method, the reader is encouraged to read that report. Rohlfing et al. tells us that in a mathematical sense, “*an atlas A is a mapping $A : \mathbb{R}^n \rightarrow \Lambda$ from n -dimensional spatial coordinates to labels from a set of classes Λ .*” In a more general sense, an atlas can be described as a type of model image that represents certain characteristics of an image population. Such an atlas can be generated for example by manual segmentation of an image or volume. Given an image, one can use a corresponding atlas in order to segment the image. This is often done through image registration, a process where different sets of data (such as two different images or volumes) are transformed to fit in a common coordinate system, often by identifying and associating similarities between the

two different sets. The atlas(es) is/are registered to an image of interest, and by identifying regions with similar characteristics to the already labelled regions in the atlas(es), the image itself can be labelled, or segmented. An example of an atlas used for segmentation of the cardiac chambers and major blood vessels can be seen in fig.2.

The segmentations used in this project were obtained from an atlas-based segmentation tool developed by Bustamante et al. [15]

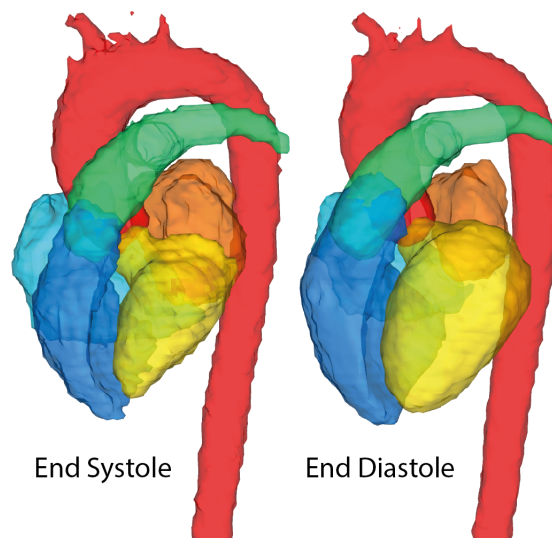


Figure 2: Example of an atlas of the human heart with six labelled regions. Red: aorta, yellow: left ventricle, orange: left atrium, blue: right ventricle, cyan: right atrium. The two images represent different time points during the cardiac cycle. Images obtained from Bustamante et al. [15, 16].

3 Theory

3.1 Hemodynamic parameters

In this section the hemodynamic parameters evaluated in this project will be introduced. This introduction will convey information about why these parameters were chosen for evaluation, and how they were calculated from the 4D Flow MRI data.

The parameters mentioned below are presented in different manners. Some are time dependant

and thus presented as a curve over time, while others are single values. Some parameters are evaluated only in certain regions of the heart, while others are calculated in all of the regions available from the segmentation. The regions are: left ventricle (LV), right ventricle (RV), left atrium (LA), right atrium (RA), aorta, and pulmonary artery.

Each parameter is in one way or another based on 4D blood flow velocity data included in the 4D Flow MR images. The velocity data consists of three 4D matrices (3D + time), each matrix containing information about the flow velocity in a certain direction. The number of time frames in each matrix is 40 (however actual time varies between data sets, depending on the heart rate of the person in question). The three directions of this coordinate system will be denoted as (x, y, z) and the corresponding velocities as (u, v, w) . Thus, the four-dimensional blood flow can be described as a time-dependent vector field V :

$$V = V(x, y, z, t) = (u(x, y, z, t), v(x, y, z, t), w(x, y, z, t)).$$

3.1.1 Speed

Blood flow speed is one of the most straightforward of the possible hemodynamic parameters to calculate and evaluate. This parameter is calculated as it is needed in order to obtain other parameters of interest. Furthermore, it is very easy to obtain, and thus there is no real reason not to include it. However, caution should be applied if considering blood speed in itself as a hemodynamic parameter. Rather, blood speed should be used in conjunction with other factors in order to obtain more meaningful information.

Given three 4D velocity matrices u, v, w the *4D Speed matrix*, S , is calculated as

$$S = \sqrt{u^2 + v^2 + w^2} \quad (2)$$

where the calculations are carried out entry-wise in the four dimensional matrix.

Blood speed was calculated in each of the six regions included, in two different manners; *average speed over time*, and *maximum speed over time*. These speeds over time for a region were calculated as the average and single maximum speed in the volume for every time frame, respectively.

3.1.2 Kinetic energy

Kinetic energy (KE) has been listed as a possible indicator for LV dysfunction [17, 18]. A slight alteration in end-diastolic LV KE for patients with mild LV remodelling has been observed, despite the fact that the LV stroke volume (which is normally used for assessing cardiac function) was unchanged [17]. This makes KE a potentially interesting parameter. Combined with the fact that it is a simple parameter to calculate, it was chosen for evaluation.

The kinetic energy for a region is calculated as

$$\text{KE} = \frac{S^2 \cdot m}{2}, \quad (3)$$

where S is the 4D speed matrix and m is the blood mass in each voxel. Blood mass is calculated as the product between the voxel volume and the blood density, chosen to be 1060 kg/m^3 . The presentation of KE as a hemodynamic parameter will be done as the sum of the KE over all N voxels for each time point, i.e.

$$\text{KE}_{\text{tot}}(t) = \sum_i^N \text{KE}_i(t), \quad (4)$$

resulting in a curve depicting *total KE over time*. Total KE was evaluated in all six regions of interest.

3.1.3 Turbulent kinetic energy

When blood flows through the heart and vessels in the body, part of the kinetic energy will be lost due to conversion into heat. This conversion can happen due to viscous friction in the vessels or cardiac chambers. As more kinetic energy is lost, the blood flow will slow down, and the heart will have to work harder in order to provide normal cardiac function [19]. As such, quantification of this loss of energy could be an indicator for certain diseases [20]. Turbulence in blood flow can be defined as irregularities and fluctuations in blood flow velocity [19]. Such turbulences in the aorta have been studied, and have been considered as a potential cause for the energy loss described above [21].

A velocity vector field can be divided into a mean and a fluctuating part, where the mean velocity field captures the average flow behaviour of the blood and the fluctuating field captures the small-scale changes. Changes due to turbulence or other irregularities will be reflected by the fluctuating field [22]. The fluctuating velocity field can then be used to calculate the Turbulent kinetic energy (TKE), a direction-independent measure of the intensity of turbulence in the blood flow. For further explanations regarding how these calculations are performed, the reader is advised to (among others) two papers by Dyverfeldt et al. [22, 23]

TKE is an interesting parameter as it has been shown to coincide with altered blood flow patterns in the aorta [24], ventricular remodelling in the right ventricle [25], as well as being prevalent in the left ventricle of patients with dilated cardiomyopathy compared to normal patients [26].

In this project, TKE was presented as *total TKE over time* (in the same manner as KE) and *max TKE over time*, which shows the maximum TKE measured in the entire region, for each time frame. TKE was evaluated for all six regions of interest.

3.1.4 Helicity

Helicity is closely related to the presence of helical flow patterns in blood. It is represented as a pseudoscalar value in each voxel, and can be said to describe the relation between blood flow strength (given by the blood flow velocity field) and the local rotation of the flow (also known as vorticity). The sign of the scalar indicates whether the flow is clockwise (positive) or counterclockwise (negative) (thus giving helicity a pseudoscalar representation). The presence of vortices in pulmonary blood flow has been shown to coincide with manifest pulmonary hypertension [27]. Furthermore, Schäfer et al. [28] states that “*there seems to be a strong correlation between helicity in the pulmonary arteries and ventricular-vascular coupling*”. Ventricular-vascular coupling is a term used to describe the efficiency of interaction between the cardiac chambers and the arterial system [29]. However, the presence of helicity is not necessarily a bad thing. Schäfer et al. [28] found that helicity was in fact lower for patients with pulmonary hypertension compared to the control group. Furthermore, they found that the ventricular-vascular coupling ratio and helicity had “*a negative curvilinear relationship*”. Helicity was also found to correlate negatively with the main pulmonary arterial pressure, and further positive correlation was found between helicity and right ventricle cardiac output [28]. All of this means that helicity is an interesting parameter to investigate, albeit a hard one to interpret.

In order to obtain helicity measurements, one first has to calculate *vorticity*, another parameter closely related to the behaviour of blood flow. Vorticity is calculated as the curl of the blood velocity vector field [19], i.e

$$\bar{\omega} = \nabla \times V = \begin{pmatrix} \frac{\partial w}{\partial y} - \frac{\partial v}{\partial z} \\ \frac{\partial u}{\partial z} - \frac{\partial w}{\partial x} \\ \frac{\partial v}{\partial x} - \frac{\partial u}{\partial y} \end{pmatrix} \quad (5)$$

Helicity density can then be calculated as [30]

$$H_d = \bar{\omega} \cdot V \quad (6)$$

In order to get the complete Helicity one would have to integrate Eq. 6 over the entire volume; however, this was not done in this project. Another helicity-related parameter is the *relative Helicity*, which is a representation of the angle between the velocity and vorticity vectors [30]:

$$H_r = \frac{H_d}{\|\bar{\omega}\| \cdot \|V\|} = \cos(\alpha) \quad (7)$$

Helicity was presented as the maximum/minimum helicity density over time, as well as mean helicity density and relative helicity over time, in all six regions. Furthermore, some values related to the max/min helicity density curves were calculated, such as the peaks of the curves, areas under the curves, quota between areas, and quota between peaks and their corresponding areas under the curves.

3.1.5 E-A wave related parameters

During the cardiac cycle, each chamber has a different blood flow pattern. For the left ventricle, the filling pattern is often analysed by looking at the speed of the blood over time. Normally this pattern contains three major blood flow speed peaks. The first one, during systole, corresponds to the emptying of the left ventricle as blood flows through the aortic valve into the aorta. The second two peaks, during diastole, are related to the filling of the ventricle, as blood flows through the mitral valve from the left atrium. Analysis of the mitral inflow pattern is a convenient way to assess cardiac function [31]. The early diastolic wave is called the E-wave, and the late diastolic wave is called the A-wave. Looking at the ratio between the E- and A-wave peak speeds, the *E/A ratio*, provides information about the cardiac function of a patient. For a healthy patient the E/A ratio is normally inside the interval $0.8 - 2$ [32]. However it should be noted that an E/A ratio within this interval does not rule out the possibility of cardiac dysfunction, as the filling pattern may be altered in ways not reflected by the E/A ratio.

Another parameter related to the E-A waves is the E-wave deceleration time (EDT), which is a measurement of how quickly the blood flow velocity decreases towards 0 after the E-wave peak. Normal EDT is around $140 - 240$ ms [32].

E-A wave related parameters have mostly been investigated for the mitral inflow of the left ventricle, and therefore that is the only region where they were evaluated in this work. Furthermore, the E/A ratio and EDT were presented as single scalar values.

3.1.6 Pressure

As the blood flow through the cardiac system is driven by differences in pressure (see section 2.1.1), pressure makes for an interesting hemodynamic parameter. For example, altered pressure during left ventricular filling at end diastole is an indicator for left ventricular dysfunction, and in the presence of stenosis (narrowing of a blood vessel), the pressure loss over the stenosis can be used as a measure of how small the narrowing is [33]. When it comes to the cardiovascular system, stenoses can occur in any of the four cardiac valves (see section 2.1.1) [34]. Pressure gradients (due to the pressure differences) are markers for cardiac dysfunction, as studies have shown a correlation between for example acute cardiac ischemia and the pressure gradients in the left ventricle [35]. Furthermore, in a study presented by Ebbers et al. [36], the pressure difference along the aortic centerline behaves differently for patients with repaired aortas, and altered pressure difference patterns between the left atrium and ventricle can be an indicator for patients with dilated cardiomyopathy.

A study performed by Eriksson et al. [33] investigated the pressure difference pattern between the base and the apex of the left ventricle of a number of healthy volunteers, providing a reference for healthy pressure behaviour in the left ventricle.

The relation between blood flow velocities and pressure gradients can be described by the Navier-Stokes equation [37]:

$$\nabla p = \mu \nabla^2 \mathbf{V} + \mathbf{F} - \rho \frac{\partial \mathbf{V}}{\partial t} - \rho \mathbf{V} \cdot \nabla \mathbf{V} \quad (8)$$

where \mathbf{V} is the blood flow velocity field, and \mathbf{F} are the body forces (caused by gravity). The calculations regarding pressure gradients and pressure values were performed using the work of a previous MSc student, Emre Kuş [38]. For further details on these calculations the reader is encouraged to read his report. In his work, Kuş also investigated and compared the pressure difference between the left atrium and the left ventricle base, as well as between the left ventricle apex and base. This was done for one healthy volunteer and a patient with dilated cardiomyopathy, and differences in the pressure pattern could be observed.

It is worth noting that the pressure fields obtained by the integration of Eq. 8 can only be determined up to an integration constant [39], which makes it a *relative pressure field*. This means that pressure gradients and pressure differences can be assessed using this method, but not absolute pressure values.

For this project, the pressure difference measurements performed by Kuş in the left hand side of the heart, as well as by Ebberts et al. [40] in the aorta were used as a foundation. For pressure calculations in the left hand side of the heart, a custom mask had to be created in order to simulate the opening of the mitral valves at the start of diastole. The mask was created as a combination of the available left ventricle and atrium masks, with the atrium part only being present during time frames corresponding to diastole. For the entirety of a heart cycle, the pressure differences were measured between the base and the apex of the left ventricle, and during diastole also between the center of the atrium and the ventricle base. For the aorta, two points along the centerline were picked out — one in the ascending and one in the descending aorta. The difference in pressure was then calculated between these two points.

Altogether, the calculated parameters related to pressure for this project were: *pressure differences over time between two points* (as described above), *maximum pressure over time*, *single peak pressure value in the region over all time frames* and *time to single peak value in the region*. For the left atrial/ventricular region, the difference between the two expected pressure difference peaks between ventricle base and apex was also calculated.

3.2 Data analysis techniques

This section will cover the theory behind the tools used to analyse the output from the hemodynamic assessment tool, when applied to a number of data sets. The output for one data set is represented as a vector, with each element describing a parameter, or an aspect of a parameter.

3.2.1 Self-organizing map

A self-organizing map (SOM), or Kohonen map as it is also called, is a type of neural network designed to visualise and analyse high-dimensional data. It is a method that is used for *unsupervised clustering*. This means that, unlike *supervised clustering methods*, it does not use any error-minimising methods in order to group the data into clusters. Supervised clustering methods compare clustering to a provided label after each training epoch. The accuracy of the clustering compared to the ground truth labels is then used as a foundation for further training. This is not the case for SOM clustering, and thus it can be performed on data without the user having to provide any labelling or background information about the data set. The SOM provides a mapping from e.g. a high-dimensional set of data onto a simpler, two-dimensional grid. Based on the available data the SOM algorithm computes a number of different models, and then associates each data set to the model best fit to describe it [41]. Each neuron of the SOM is associated with one model. Furthermore, neighbouring neurons in the SOM describe models that are similar to one another, and thus the topology of the input data is preserved.

A Kohonen map is used for the statistical analysis of parameters described in Section 1.1. In the rest of the report, the abbreviations SOM and SOFM (self-organizing feature map) will be used interchangeably.

3.2.2 Bayes' theorem

Bayes' theorem describes the probability of an event occurring, given some prior knowledge about related events. The theorem states the following:

$$P(A|B) = \frac{P(A) \cdot P(B|A)}{P(B)}. \quad (9)$$

Here, A and B are two separate events. Bayes theorem answers the question “What is the probability of the event A occurring, if I know that the event B is true?”. If the events A and B are related, then Bayes' theorem can be used to better assess the probability of the event A given knowledge about B, compared to not using any prior information about B. This is useful for this work, as it may provide us with information regarding the probability of a data set having a certain medical condition given the characteristics of its corresponding hemodynamic parameters.

3.2.3 Feature scaling

Feature scaling is used to standardise values in e.g. a data vector into a certain range. The simplest version of this is to normalise the data into the range [0, 1]. This is done by subtracting

the minimum value of a vector X from each element in X , and then dividing each element by the difference between the largest and smallest elements. The formula for this is

$$X' = \frac{X - X_{min}}{X_{max} - X_{min}} \quad (10)$$

where X is the original data vector and X' is the data vector after scaling.

This is useful for us as the size range between parameters of the output we are dealing with differ greatly.

4 Methods

4.1 Study population

The study population was composed of healthy volunteers as well as patients with different degrees of cardiac disease, including aortic and mitral regurgitation, left ventricular hypertrophy, aortic stenosis, ischemic cardiomyopathy, dilated cardiomyopathy and diastolic dysfunction. The tool was successfully applied to 117 different data sets, corresponding to subjects between the ages of 30 and 84. The mean age of the study population was 65 ± 9 years. The distribution of gender was 78 males and 39 females.

4.2 Acquisition settings

The MRI examinations were performed on a clinical 3T Philips Ingenia scanner (Philips Healthcare, Best, the Netherlands). Prior to the acquisition all subjects were injected with a Gadolinium contrast agent (Magnevist, Bayer Schering Pharma AG) for a late-enhancement study. 4D Flow MRI examinations were performed during free-breathing, using a navigator gated gradient-echo pulse sequence with interleaved three-directional flow-encoding and retrospective vector cardiogram controlled cardiac gating. Scan parameters included: Candy cane view adjusted to cover both ventricles, velocity encoding (VENC) 120-150 cm/s, flip angle 10° , echo time 2.5-2.6 ms, repetition time 4.2-4.4 ms, parallel imaging (SENSE) speed up factor 3 (AP direction), k-space segmentation factor 3, acquired temporal resolution of 33.6-52.8 ms, spatial resolution $2.7 \times 2.7 \times 2.8 \text{ mm}^3$, and elliptical k-space acquisition. The 4D Flow MR images were corrected for concomitant gradient fields on the MRI scanner. Offline processing corrected for phase wraps using a temporal phase unwrapping method [43], and background phase errors were corrected using a weighted 2nd order polynomial fit to the static tissue [44].

4.3 Implementation details

This section contains information regarding the calculation of some of the parameters included in the hemodynamic assessment tool. The tool was created using MATLAB (Release 2016a, The MathWorks, Inc., Natick, Massachusetts, United States).

4.3.1 Finding systole/diastole

One of the challenges encountered was finding a robust way of determining which time frames correspond to which phase in the cardiac cycle. We know that at the start of systole there is a lot of blood in the ventricles which is then pumped out through the aorta. This makes the blood speeds in the aorta suitable for determining the peak systolic time frame. Determining exactly when systole ends and diastole begins is a more difficult task. However, for this project, it was enough to estimate an approximate location of this phase. A reasonable assumption is to mark the end of systole at a time frame slightly ahead of the peak systolic speeds in the aorta. Information about the end of systole was used for the calculation of E/A related parameters as the time points of interest occur during diastole (see Section 3.1.5), as well as for creating the custom mask used for pressure difference calculations between the atria and ventricles (see Section 3.1.6).

When analysing the data, knowing which time-frames correspond to peak systole and diastole is useful, as explained in Section 4.4.1. The average blood speeds in the left ventricle (LV) were used to calculate these. As described in Section 3.1.5, the LV flow pattern contains three major blood flow speed peaks — one in systole and two in diastole. The two diastolic peaks correspond to the early and late ventricular filling. As these time frames were to be used for post analysis processing, it was important to ensure that they could be reliably said to represent the same time points in the cardiac cycle in different data sets. *LV average speeds* follow a quite established pattern, and were thus used for these calculations. Using the previously determined time frame of the end of systole, the LV average speeds could be divided in two. Then, the time frames corresponding to the two largest peaks in diastole and the largest peak in systole were found.

Since the input data may contain abnormal patterns, measures were taken to ensure the robustness of the tool. These measures include the exclusion of peaks whose values are too small, or peaks that are not wide enough. If any abnormalities are encountered during calculations, the tool provides the user with a warning, so that the outcome may be verified manually. An example showing the LV average speed for one data set and the corresponding time frames of the calculated blood flow peaks can be seen in Fig. 3.

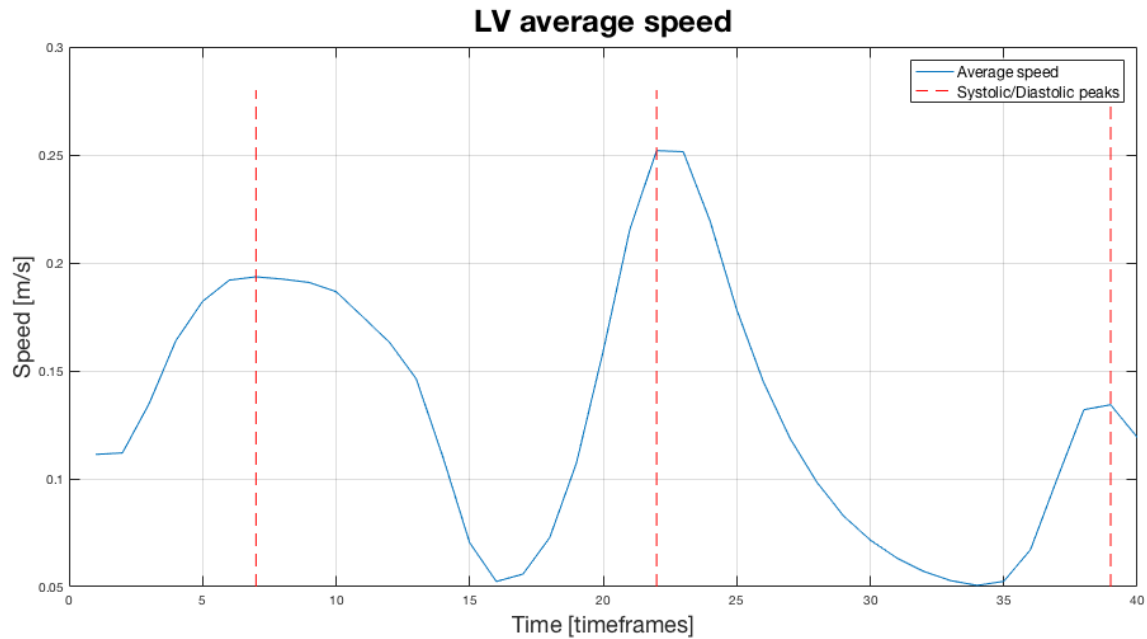


Figure 3: The average speed in the left ventricle (LV) over time (blue) and the calculated time frames corresponding to the systolic (first) and diastolic (second and third) peaks (red) for one data set.

Using the information about systolic and diastolic peaks in conjunction with the time frame corresponding to the end of systole also lets the tool deal with potential time shifts in the data. Such a time shift might mean that for a data set, the time frames corresponding to diastole occurs before systole. In such a case the time frames corresponding to the LV average speed peaks will be located before the end of systole. The tool will capture this behaviour, warn the user, and shift all of the original data in time, and redo the analysis.

4.3.2 Pressure difference

As explained in Section 3.1.6, the pressure difference parameters were obtained as the difference between several sets of pairwise points. The location of these points needed to be determined in a proper way, and the methodology behind that is explained in this section.

For the left and right side of the heart, there were three points of interest; one in the atrium and two in the ventricle. The two ventricular points were to be located at the base and apex of the ventricle. The main challenge regarding these points is the fact that over time the cardiac chambers expand and deflate and thus the cardiac walls are subject to a lot of movement. Thus, the tool needed to be able to adapt in case a point in space previously calculated as, for example, the estimation for the base of the left ventricle, suddenly ended up outside of the

heart due to ventricular movement.

The atrial points were obtained as the average centroids of the atria over time. As it is mostly the chamber walls that are subject to movement, the average centroid should not differ much from the centroid at each time frame. In order to obtain the ventricular apex and base coordinates, the ventricular centroids were obtained in the same manner as for the atria. A directional vector between the atrial and ventricular centroids was calculated. To determine the base and apex coordinates the tool “walks” through the atrial and ventricular masks for an arbitrary time frame, along the vector between centroids. After each step it checks if it has yet entered the ventricular mask. Once it has, it progresses a few more steps along the centroid vector and sets those coordinates to be the ventricular apex. For the points corresponding to the ventricular base, the tool keeps walking along the directional vector between the two centroids. After each step, the tool checks if it has left the ventricular mask. When the mask has been left, the tool backtraces a couple of steps along the line, and picks that point as the ventricular base. These points were then used for the calculations. Since the ventricular mask moves over time, there is a risk that the calculated base and apex points may end up outside of the mask. Should this happen at any point, the tool automatically recalculates the points in the current time frame, and proceeds by using these new coordinates instead.

For the aorta, the locations of interest were in the ascending and descending aorta. In order to find these points, a MATLAB function written by Kollmannsberger et al. [42] was used. Provided a binary 3D aortic mask, the function `skel2graph` makes a conversion into a network graph described by nodes and edges. By pruning the network graph to get rid of smaller branches, the main centerline of the aorta could be found, and two points were chosen at the edges of this centerline. In the same manner as for the atrial/ventricular pressure difference, the tool recalculates the points and warns the user in case the points end up outside of the mask at some point.

4.3.3 Obtaining and visualising results

Once applied to a 4D Flow MRI data set, the tool outputs a file with all of the calculated parameters, as well as 4D-matrices describing the behaviour of some of the parameters in the entire region. These parameters are helicity density, relative helicity, kinetic energy, and the pressure fields. Used in conjunction with segmentations of the cardiac chambers, these 4D-matrices can clearly illustrate the behaviour of one of the previously mentioned parameters over the cardiac cycle. The custom masks created for pressure difference calculations in the atria/ventricles are also saved. Any generated warnings or error messages displayed during analysis are saved to a log file in order to facilitate troubleshooting.

If analysis has already been performed on a data set, the tool instead offers the possibility to plot all of the time-dependent parameters. Furthermore, the tool provides means to calculate a set of average parameters from a number of data sets, as well as the option to create meaningful plots that clearly illustrate differences between an arbitrary data set and a group of data sets

with similar characteristics.

4.4 Post-processing of results

The finished tool was used on a number of data sets. This section describes the data sets on which the tool was applied, and how it was done.

4.4.1 Comparison between data sets

A large point of interest, and a potential main usage point for this tool is the ability to compare parameters between data sets. However, the velocity data is evaluated over the course of one heart beat, and this time scale is not necessarily exactly the same in different data sets due to variations in heart rate. For example, for one arbitrary data set A, the peak systolic time frame (as described in section 4.3.1) might be 10 (out of 40), whereas for another data set B, the corresponding time frame might be number 13. When comparing data set A and B, it then makes little sense to compare time frame 10 in A to time frame 10 in B, and vice versa. Thus, a method to be able to perform automatic comparison between two data sets with different time scales had to be developed.

As explained in section 4.3.1, the three major blood flow speed peaks in the left ventricle are good indicators of different time points during the cardiac cycle. During the analysis of data, along with all of the parameters, the hemodynamic assessment tool also saves the calculated time frames of these three peaks. These peaks play a major part in the process of making data sets comparable to each other.

It could be interesting to calculate a set of “average parameters”, for example from a group of data sets corresponding to healthy volunteers. However, for the average parameter set to make sense, we first have to make sure that the data sets included in the average are on the same time scale. It makes little sense to take an average at a time frame if the time frame in question does not represent the same time point in the cardiac cycle for different data sets. This can clearly be seen by looking at Fig. 4. There, curves representing the LV average speeds for a number of healthy volunteers are seen. The location of the average systolic and diastolic peaks from all data sets corresponding to healthy volunteers are also marked. The number of healthy volunteers included in this average is greater than three, but for illustrative purposes, only three speed curves are shown.

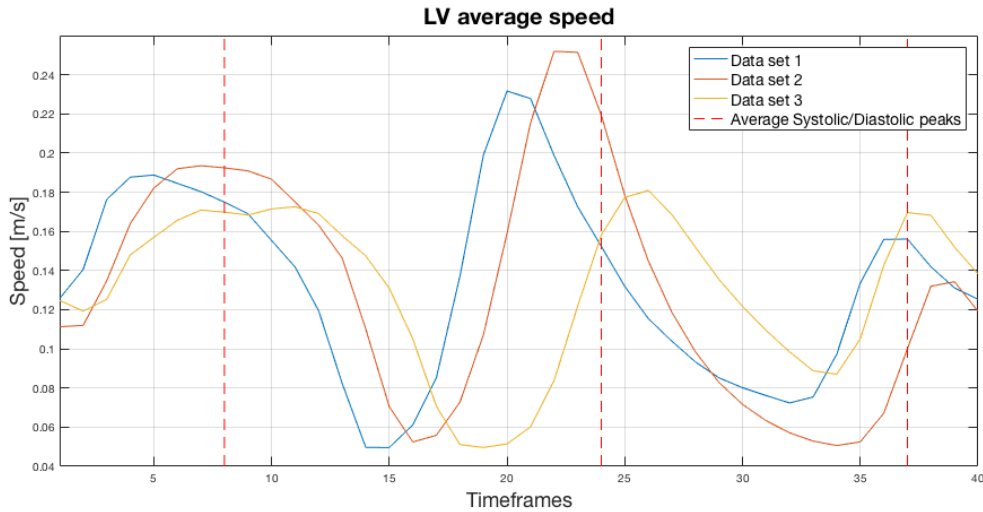


Figure 4: The average speeds in the left ventricle for three data sets corresponding to healthy volunteers (blue, orange, yellow) with the average locations of the systolic and diastolic peaks marked (red, dashed).

It is easily observed that the location of the systolic and diastolic peaks of the three data sets do not coincide with the location of the average peaks. Thus, the parameters of each of the data sets to be included in the average need to be shifted, so that the peaks do coincide with the average set. This is done by first skewing all of the data points in each set before the first peak so that the locations of the systolic peaks coincide. This is done by finding a factor k equal to the quota between the average systolic time frame and the time frame of the systolic peak of each data set. Each time frame before and including the systolic peak is then multiplied by this factor k . Next, the data points after the second diastolic peak are skewed in the same manner, with regards to the second diastolic peak. Finally, the points between the first diastolic peak and the two other peaks are skewed linearly between peaks. This does however make it so that the time frame scales of the data sets are no longer the original $[1, 2, \dots, 39, 40]$. Thus, the data has to be interpolated onto any missing time frames (using the MATLAB function `interp1`), and thereafter reevaluated onto the original time frame scale.

In order to align every single parameter in the average parameter set, interpolation is performed on all of the data sets, using the new time frame scale obtained from the LV average speeds. With all of the parameters in all of the data sets aligned to the average systolic and diastolic peaks, the mean and standard deviation of the parameter curves could be obtained in each time frame. One example of such a plot is shown in Fig. 5.

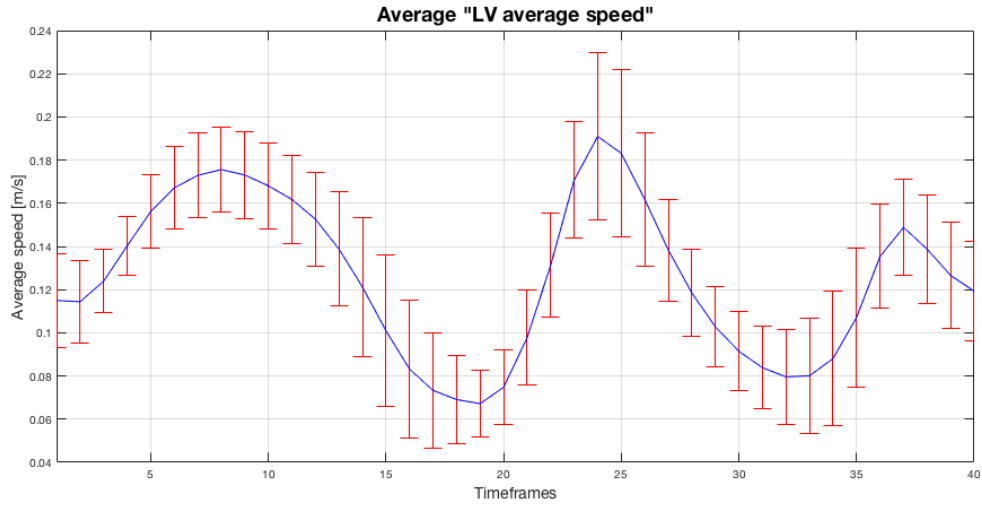


Figure 5: The average speeds in the left ventricle (LV) for the average parameter set consisting of healthy volunteers. The blue line shows the mean, and the red bars the standard deviation.

The same principle as above is applied when comparing the parameters of an arbitrary data set (denoted as S_{arb}) to the average parameter set (denoted as S_{avg}). S_{avg} is obtained by the methodology described above, and is an average parameter set obtained from data sets which we know correspond to healthy volunteers. It could be interesting to compare S_{arb} to S_{avg} in order to assess if there are any noteworthy differences between them.

However, to be able to compare S_{avg} and S_{arb} time frame by time frame, the curves first have to be on the same time scale. By plotting the LV average speeds for the single patient in the same image as the group average, we can draw the conclusion that a direct comparison between the two would make little sense (Fig. 6).

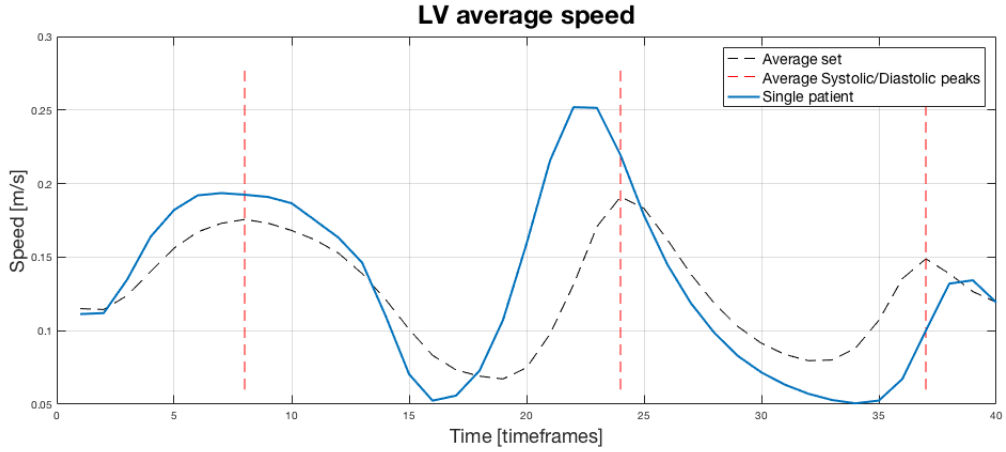


Figure 6: The average speeds in the left ventricle for S_{avg} (black, dashed), and the arbitrary patient S_{arb} (blue), with the locations of the average systolic and diastolic peaks marked (red, dashed).

In the same manner as for the creation of S_{avg} described previously, the LV average speed of S_{arb} was skewed so that the locations of the systolic and diastolic peaks between S_{arb} and S_{avg} coincide. The result can be seen in Fig. 7.

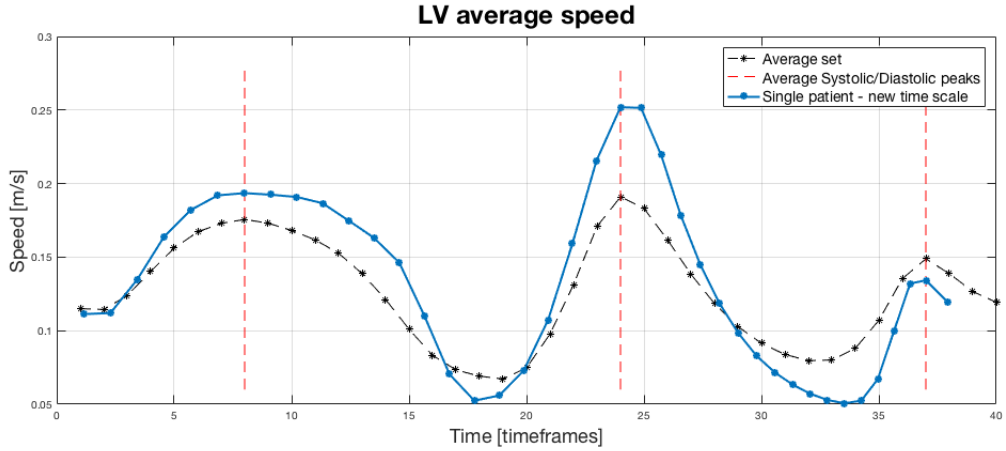


Figure 7: The average speeds in the left ventricle for S_{avg} (black, dashed), and the arbitrary patient S_{arb} (blue) after shifting its curve to coincide with S_{avg} . The points on the lines show the locations of the time frames where the data is evaluated. The locations of the systolic and diastolic peaks are marked (red, dashed).

As can be seen in Fig. 7, the systolic and diastolic peaks of S_{avg} and S_{arb} now coincide. However, since the time points of S_{arb} have been shifted, its data points are rather evaluated at slightly different locations, for example $T_2 = [1.1, 2.2, \dots, 37, 38.1]$ (with the total number

of data points still remaining 40). Thus, the last step to make S_{arb} and S_{avg} comparable is to interpolate S_{arb} at the original time frame positions ($T = [1, 2, \dots, 40]$). The final result can be seen in Fig. 8.

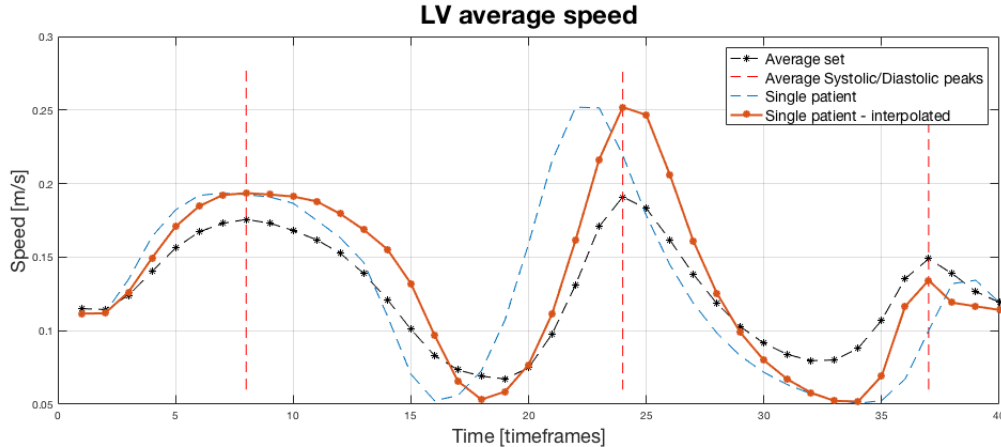


Figure 8: The average speeds in the left ventricle for S_{avg} (black, dashed), the arbitrary patient S_{arb} before (blue, dashed) and after (orange) interpolation. The points on the lines show the locations of the time frames where the data is evaluated. The locations of the systolic and diastolic peaks are marked (red, dashed).

As can be seen in the figure above, the blue and orange lines still have the same characteristics; however, their peaks are now aligned. Furthermore, the location of the data evaluation points (time frames) are the same between the orange and the black curve. Thus, the curves in data sets S_{avg} and S_{arb} can now be compared quantitatively in a way that makes sense.

4.4.2 Data analysis

With the finished tool in hand and applied to a number of data sets, the next point of interest was to evaluate the parameter outputs to see if any correlation could be found between certain parameters and some data set labelling not included in the tool. Such a labelling could be for example the severity of disease of the data sets, age, gender etc.

Most of the parameters obtained are curves over time, and to make these easier to analyse quantitatively, each curve was instead represented as three discrete values. These values were obtained as the curve values at the systolic and two diastolic peaks (as described in section 4.3.1). After splitting up each time dependent parameter into three discrete values, the total number of different parameter values per data set was 235. These parameter values were arranged in a matrix where each row corresponded to one data set, and each column to a parameter. The idea was to use an unsupervised learning method to divide the 117 data sets into different clusters depending on their characteristics determined by the parameter values.

Once such a clustering had been obtained, the inference of each data set could be compared to some external label. This would provide us with information regarding the viability of the hemodynamic parameters used as a divider between different groups of data sets.

Clustering was performed using MATLAB’s implementation of self-organizing feature maps (SOM) to divide the data into clusters. However, since the order of magnitude between the parameters differ greatly and each parameter corresponds to a different unit, feature scaling (eq. 10) was performed on each column (parameter) of the data matrix. This way, parameters with different units could be compared to one another. The size of the SOM grid was set to be 2 by 2, allowing for four different clusters. After clustering the data, the groups obtained could be compared to some external label to investigate possible correlation between said label and the clustering based on hemodynamic parameters. The chosen label for this was left ventricular ejection fraction (EF, see 2.1.3). For the data sets in question, EF had already been calculated from manual heart segmentations performed for a previous study. Data sets were split into two groups depending on their EF. One group (labelled as group 1) had an EF below 50%, and the other (group 2) had an EF above or equal to 50%. The number of data sets in each labelled group was 30 and 87, respectively. The EF labelling of the data sets was then compared to the cluster inferences. The ratio of cluster belongings for the group of data sets corresponding to each of the two labels, enabled the calculation of posterior probabilities regarding the labels. These calculations were performed using Bayes’ theorem (Eq. 9) as

$$P(L_i|C_j) = \frac{P(L_i) \cdot P(C_j|L_i)}{P(C_j)}.$$

This answers the question “what is the probability of an arbitrary data set having the label L_i (i.e. EF below or above 50%) if it belongs to the cluster C_j ?”. Here, $P(L_i)$ is the fraction of all data sets with the label L_i . $P(C_j)$ is the fraction of data sets belonging to the cluster C_j . $P(C_j|L_i)$ is the fraction of data sets with the label L_i belonging to cluster C_j .

5 Results

5.1 Parameter visualisations

5.1.1 A single data set

In this section, all of the plots obtained from the hemodynamic assessment tool when applied to a single data set are presented. The data set in question belongs to a healthy volunteer.

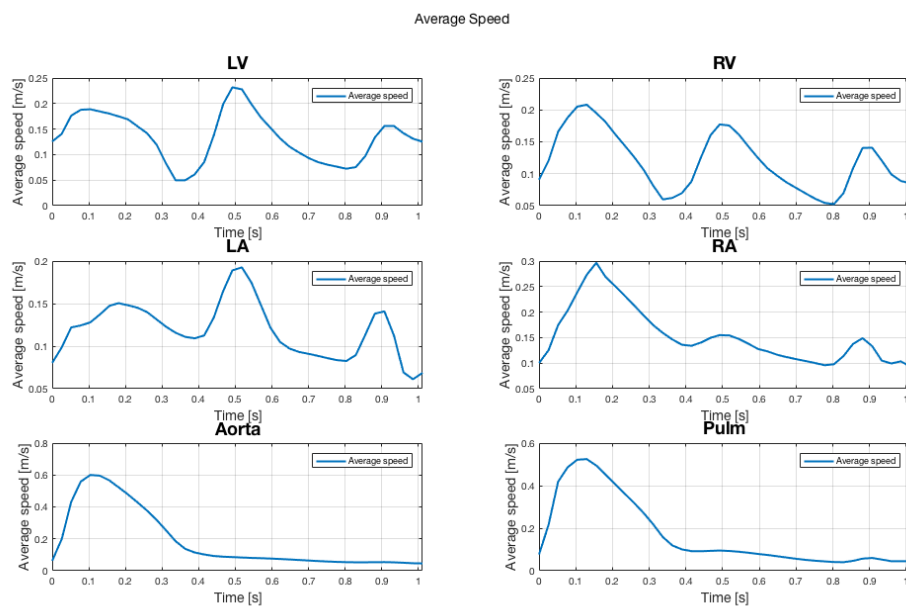


Figure 9: Average speed [m/s] over time [s] of a single data set for six different regions.

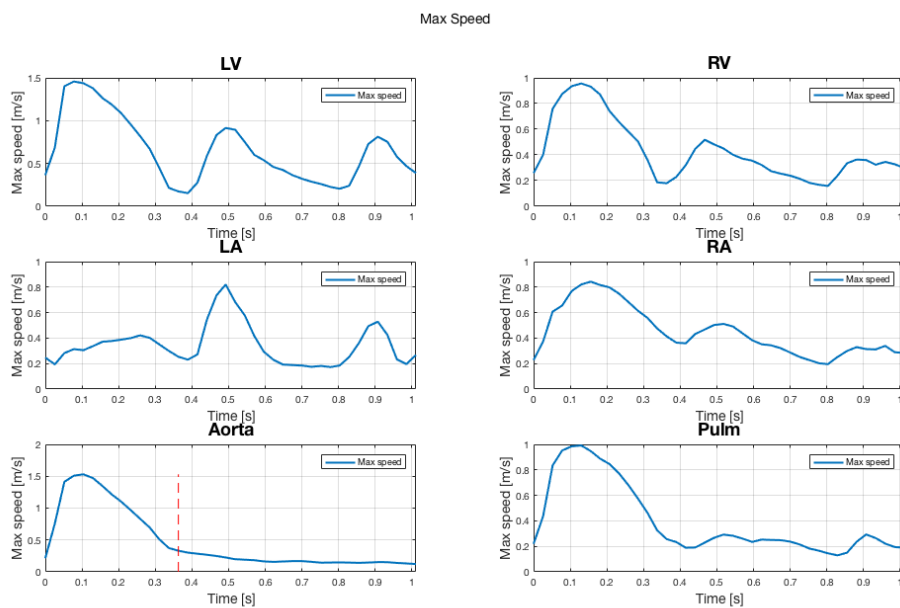


Figure 10: Maximum speed [m/s] over time [s] of a single data set for six different regions. The red dashed line in the bottom left plot marks the end of systole.

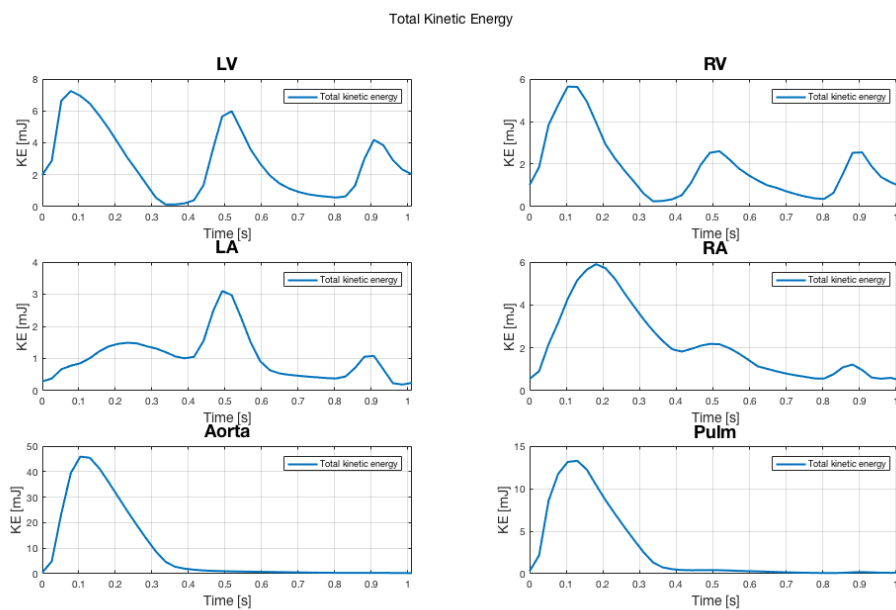


Figure 11: Total kinetic energy [mJ] over time [s] of a single data set for six different regions.

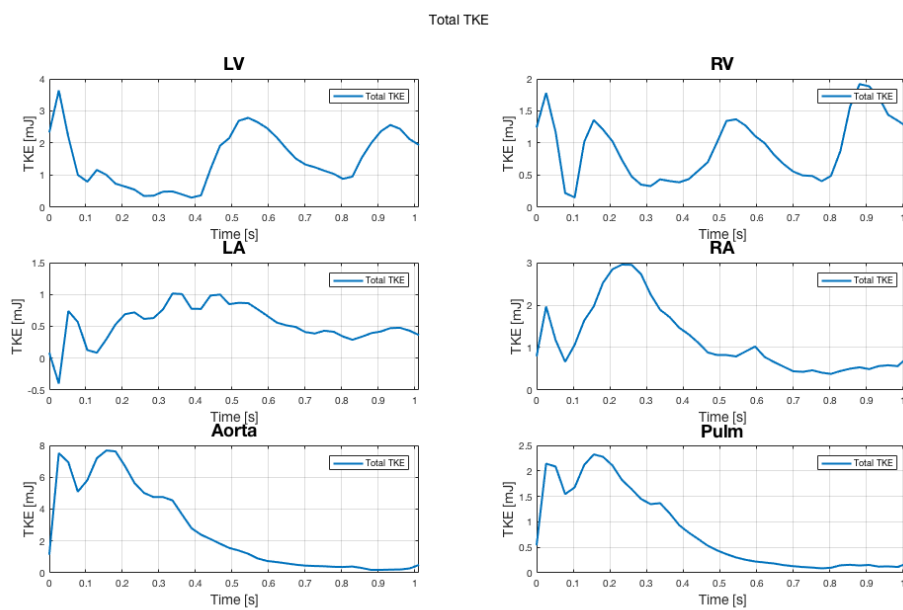


Figure 12: Total turbulent kinetic energy [mJ] over time [s] of a single data set for six different regions.

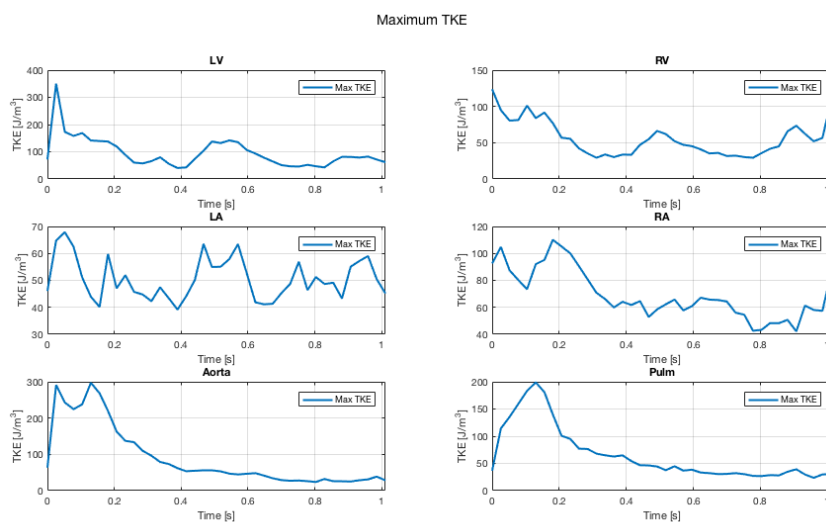


Figure 13: Maximum turbulent kinetic energy [J/m^3] over time [s] of a single data set for six different regions.

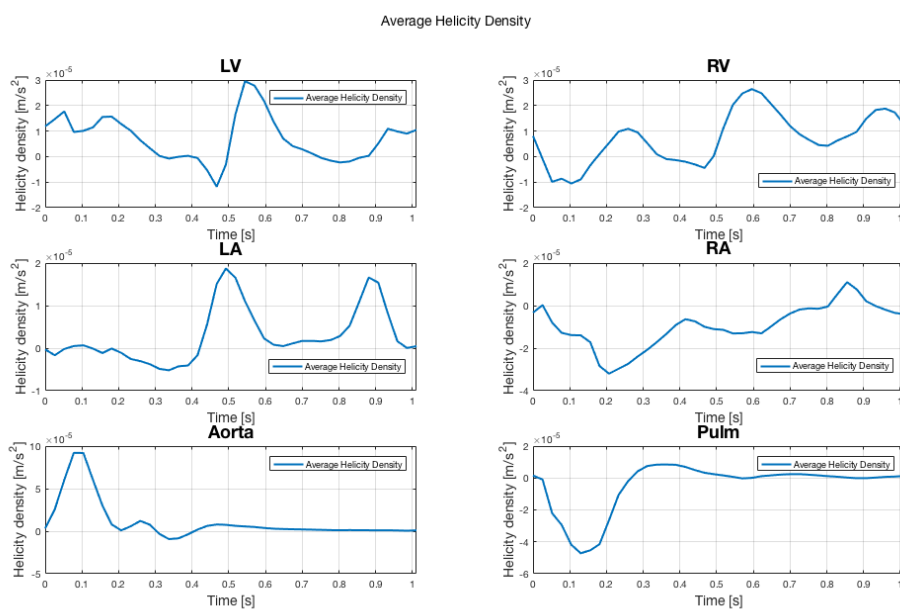


Figure 14: Average helicity density [m/s^2] over all voxels over time [s] of a single data set for six different regions.

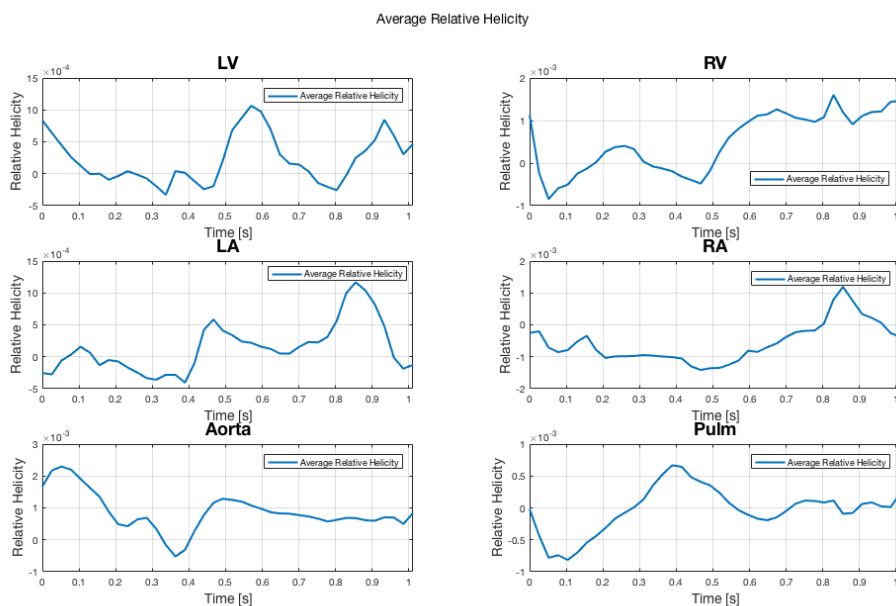


Figure 15: Average relative helicity over all voxels over time [s] of a single data set for six different regions.

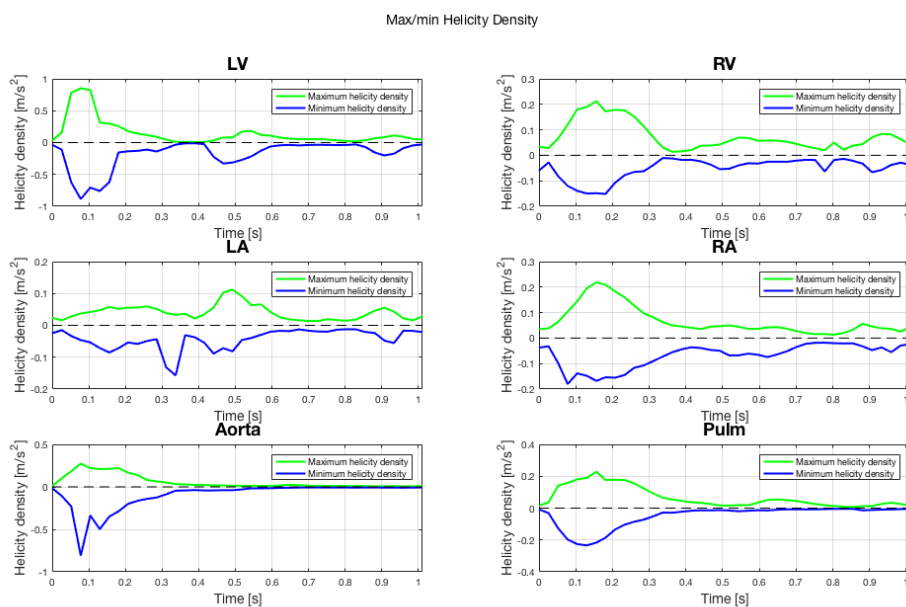


Figure 16: Maximum (green) and minimum (blue) helicity density [m/s^2] over time [s] of a single data set for six different regions.

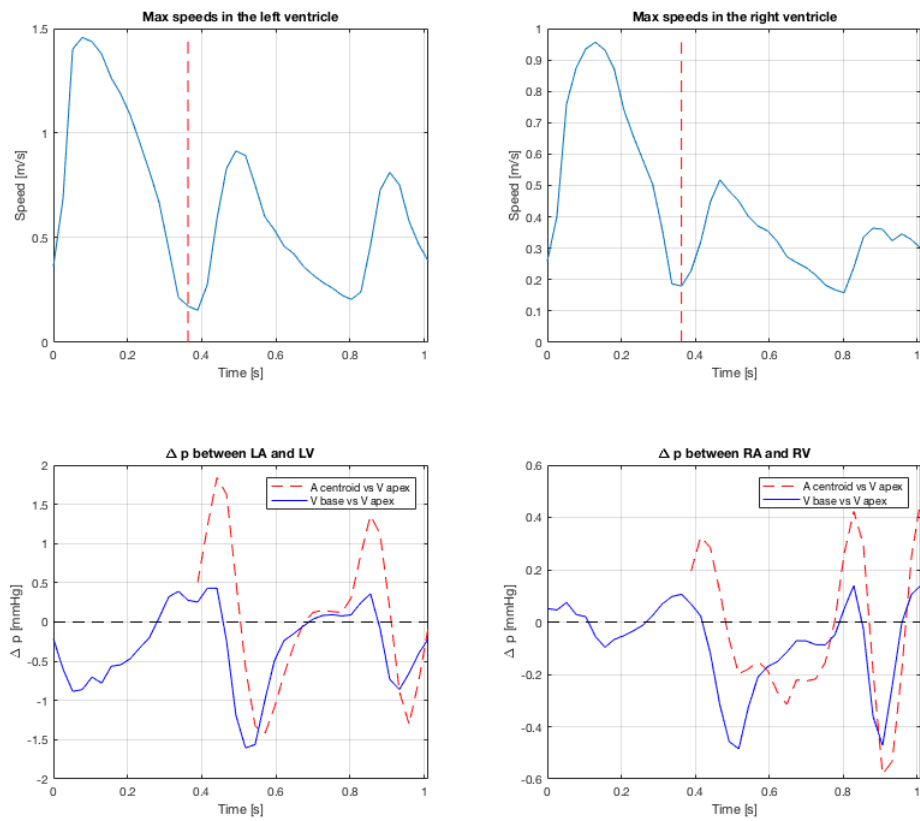


Figure 17: Pressure differences [$mmHg$] between atria and ventricles (bottom, left atrium/ventricle to the left, right atrium/ventricle to the right) over time [s]. Blue lines show pressure difference between ventricle base and ventricle apex, red dashed lines show pressure differences between atrium centroid and ventricle base. The top two images show the max speeds in the corresponding ventricles for reference. The vertical red dashed lines there mark the end of systole.

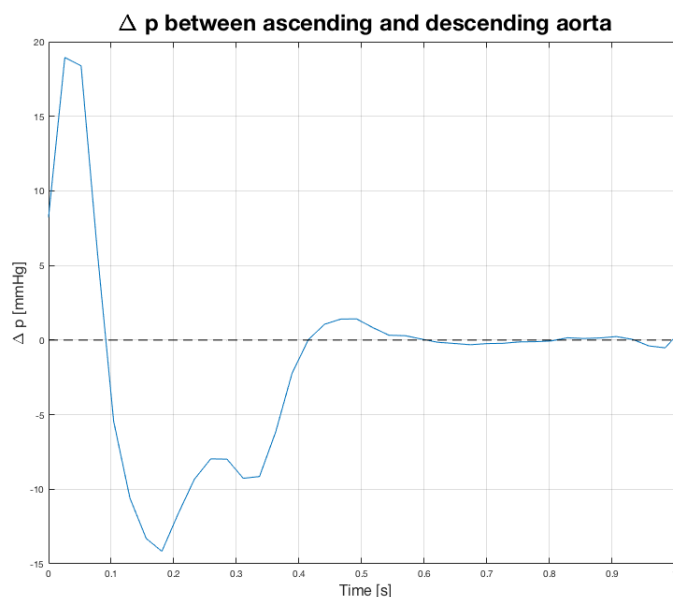


Figure 18: Pressure difference [$mmHg$] between the ascending and descending aorta over time [s] of a single data set

The single parameter values obtained from the tool are presented in tables 1 and 2. For this data set the E/A ratio was 1.1262, and the EDT 0.3110 s .

Parameter/Region	LV	LA	RV	RA	Aorta	Pulm
Maximum H_d peak	0.8526	0.1119	0.2126	0.2186	0.2730	0.2286
Maximum H_d curve area	5.8383	1.6216	2.9410	2.6636	2.3326	2.6557
Minimum H_d peak	-0.8863	-0.1574	-0.1514	-0.1800	-0.8086	-0.2341
Minimum H_d curve area	7.2266	1.7397	2.0671	2.7463	3.8463	2.0054

Table 1: The single parameter values related to the maximum/minimum helicity density curves.

Parameter/Region	L A/V	R A/V	Aorta
Peak pressure [mmHg]	1.3599	1.1624	11.4343
Time to peak pressure [s]	0.4670	0.3370	0.1810
Difference between Δp peaks [mmHg]	0.0710	-	-

Table 2: The single parameter values related to the pressure in the left/right atrium/ventricle and aorta.

5.1.2 Volume renderings

In addition to the plots presented above, helicity density, turbulent kinetic energy, kinetic energy and blood flow velocities can be presented as a volume render over all time frames. In Figs. 19 and 20 these are presented at the time frames corresponding to peak systole, early and late diastole.

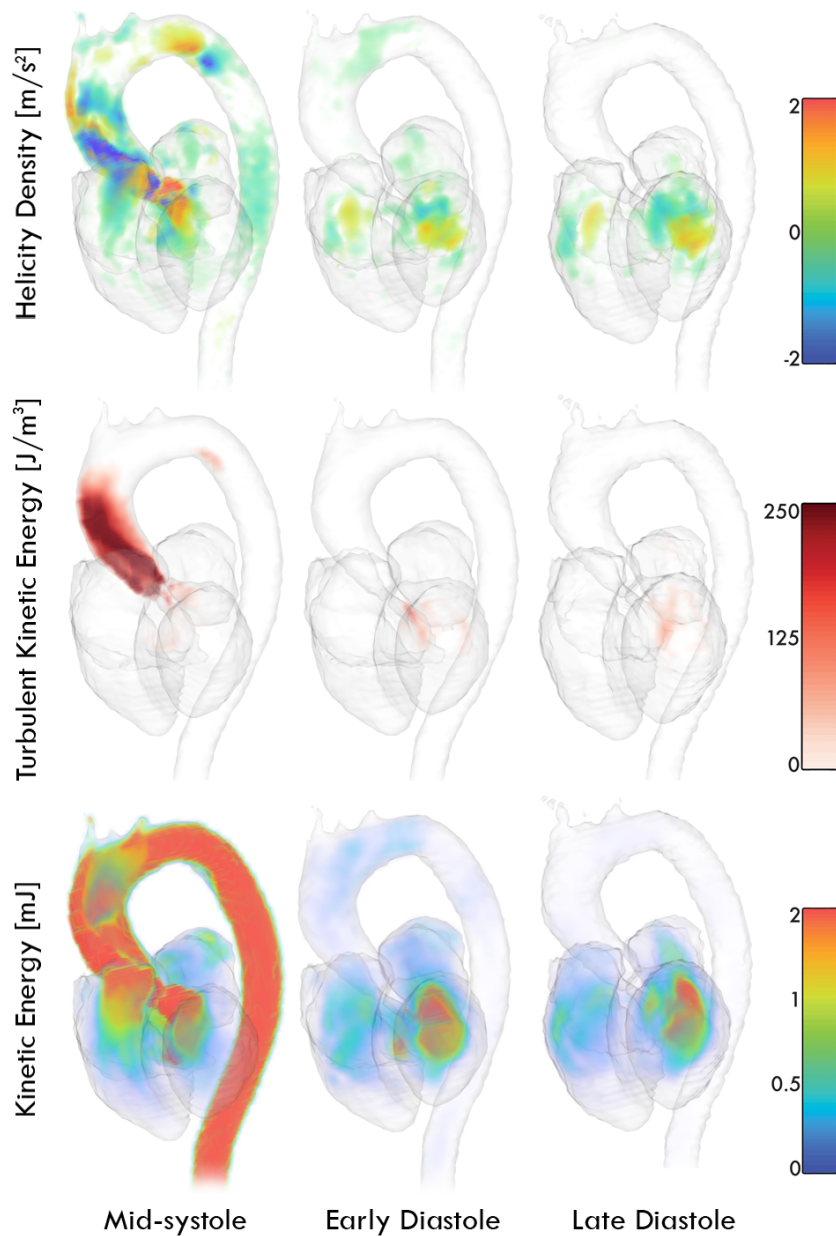


Figure 19: Helicity Density, Turbulent Kinetic Energy and Kinetic energy visualised as volume renders. The data set corresponds to a patient with aortic valve stenosis.

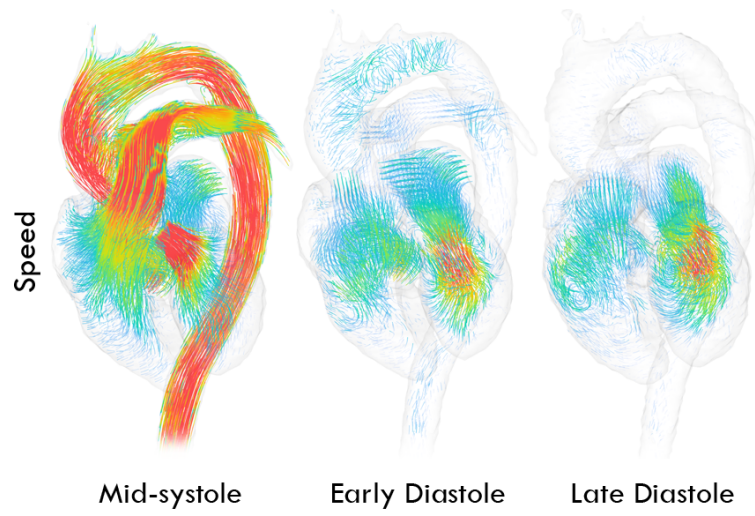


Figure 20: Blood speed visualised as streamlines. The data set corresponds to a patient with aortic valve stenosis.

5.1.3 Average curves - example

Two examples are provided of how the average curves are presented. The principle is the same for all the different parameters. The average curves presented below correspond to a group of 12 healthy volunteers.

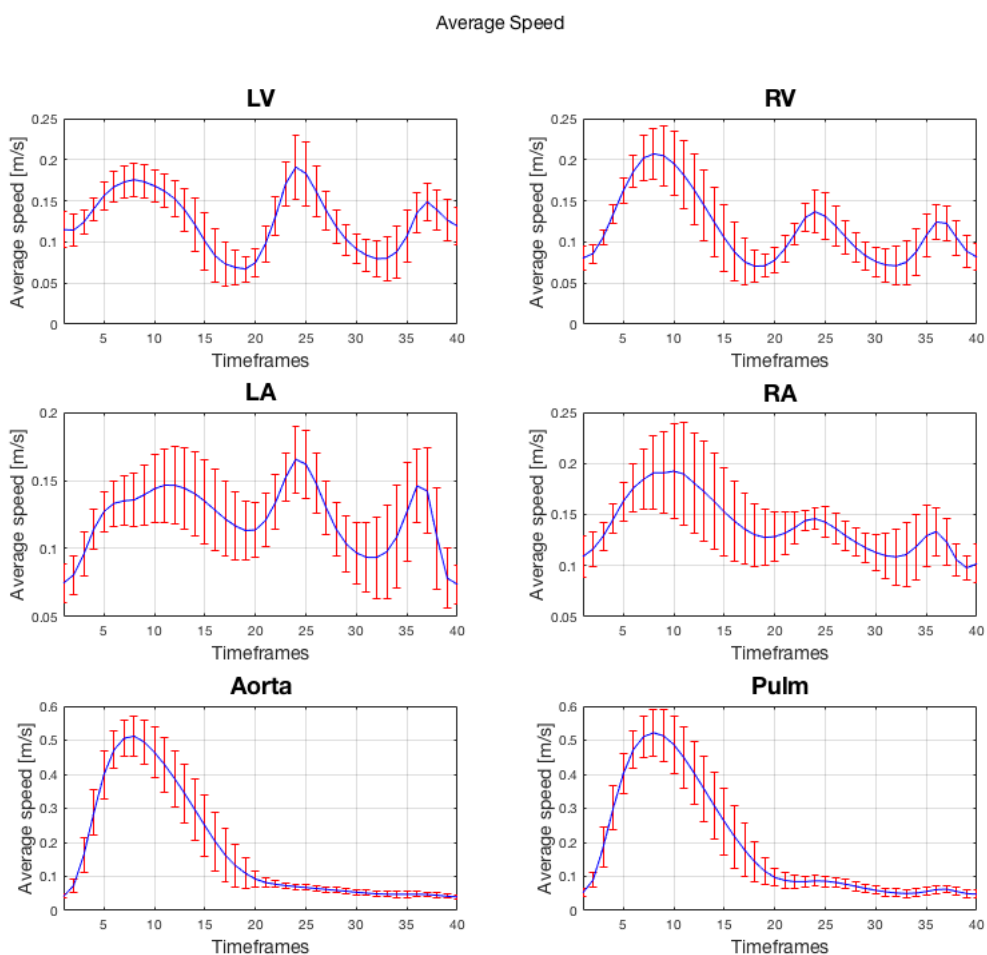


Figure 21: Average speed [m/s] over time averaged from twelve data sets corresponding to healthy volunteers. The blue curves show the mean for each region, and the red bars show the standard deviation at each time frame.

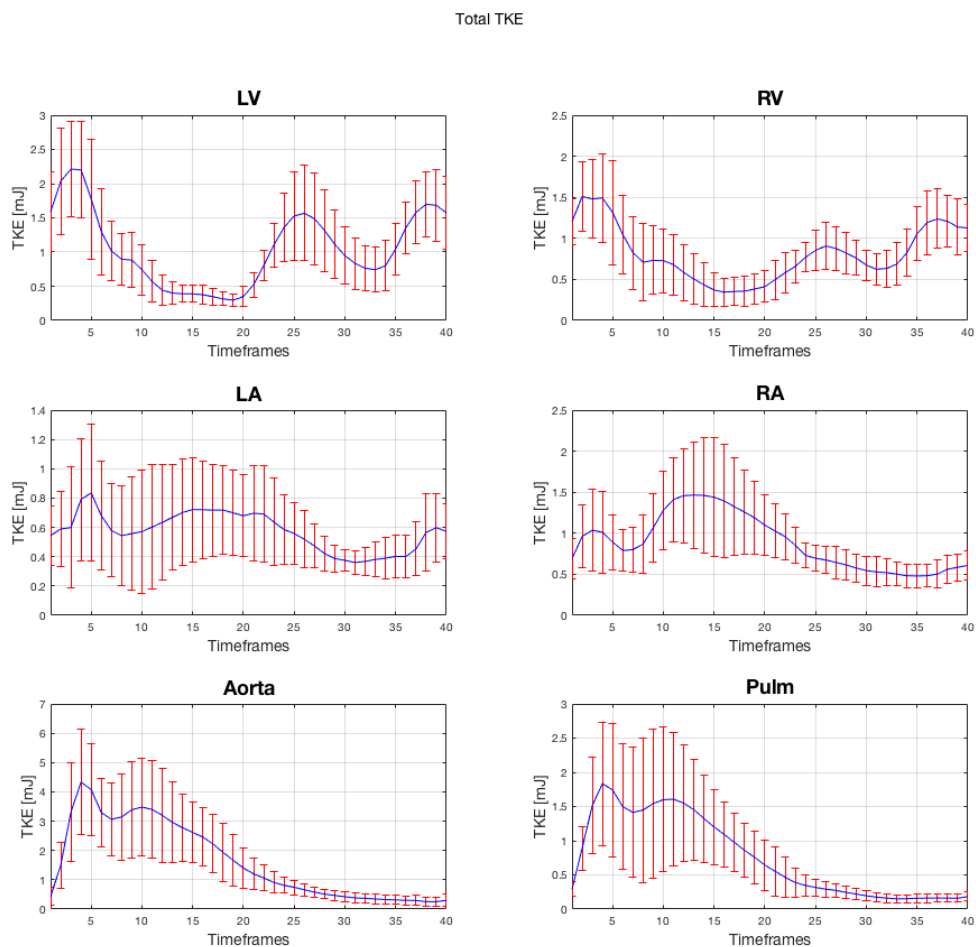


Figure 22: Total turbulent kinetic energy [mJ] over time averaged from twelve data sets corresponding to healthy volunteers. The blue curves show the mean for each region, and the red bars show the standard deviation at each time frame.

5.1.4 Comparison between a patient and average healthy data sets

Here, the comparisons of the average speeds and total turbulent kinetic energy between a patient with aortic valve stenosis and the average healthy parameter set are shown.

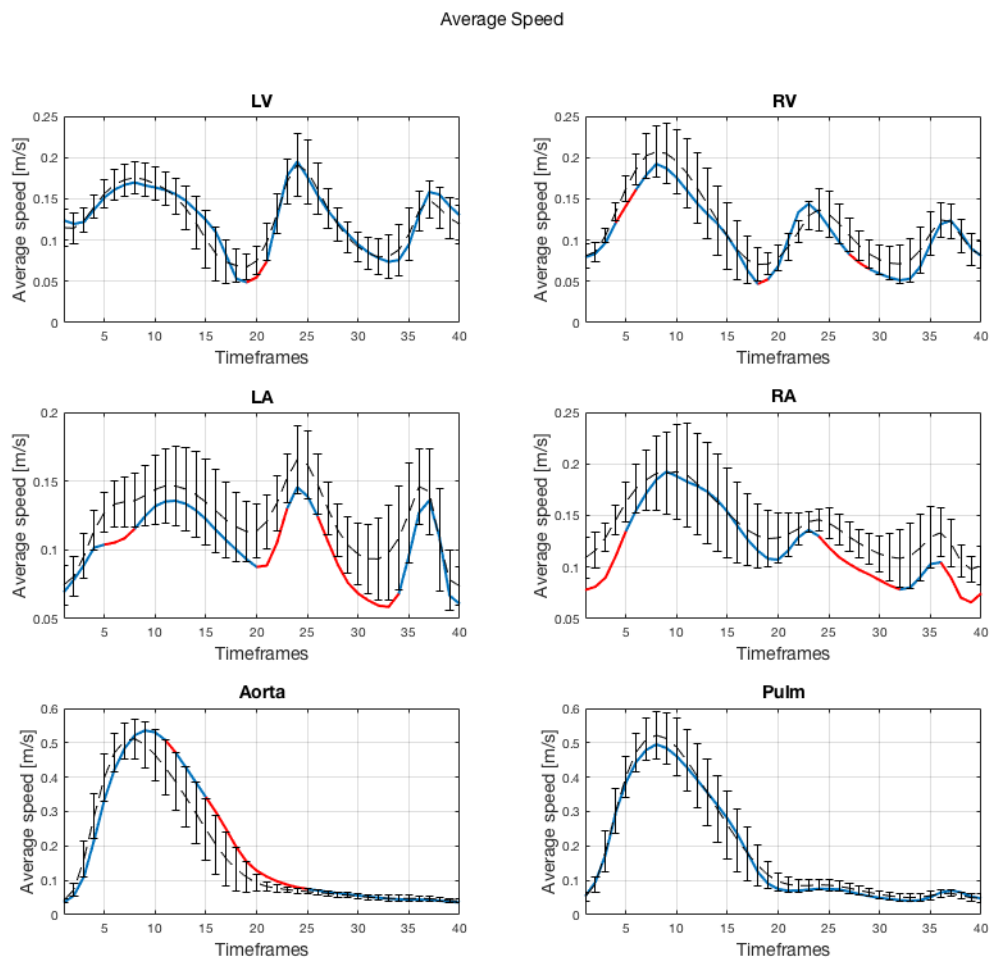


Figure 23: Average speed [m/s] averaged from twelve data sets corresponding to healthy volunteers (black, dashed), compared to the average speed of a patient with aortic valve stenosis (blue and red). The blue parts of the curves represent time frames where the curve value for the patient is within the standard deviation of the mean for the average curves, and the red parts where the values are outside of this interval.

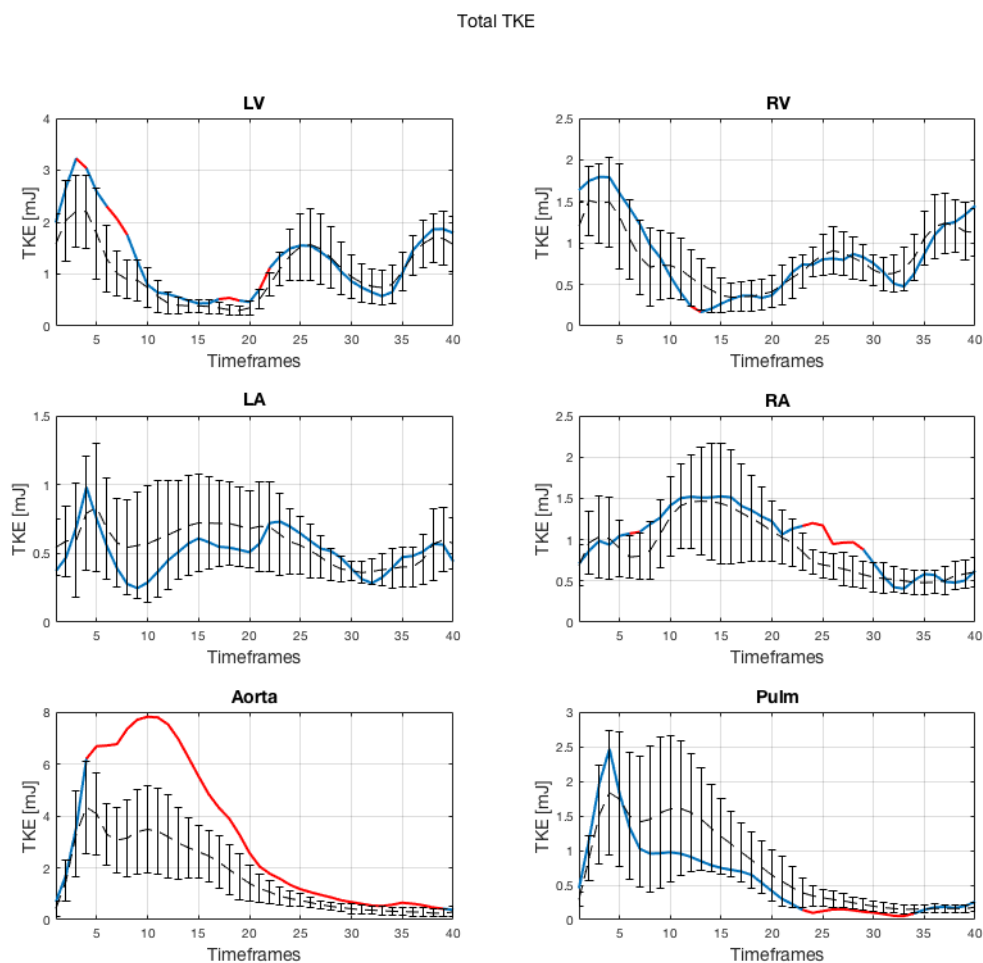


Figure 24: Total turbulent kinetic energy $[mJ]$ over time averaged from twelve data sets corresponding to healthy volunteers (black, dashed), compared to the total TKE of a patient with aortic valve stenosis (blue and red). The blue parts of the curves represent time frames where the curve value for the patient is within the standard deviation of the mean for the average curves, and the red parts where the values are outside of this interval.

5.2 SOFM Clustering

In this section the clustering, and different pieces of information related to this, obtained from MATLAB's self-organizing map neural network tool is presented.

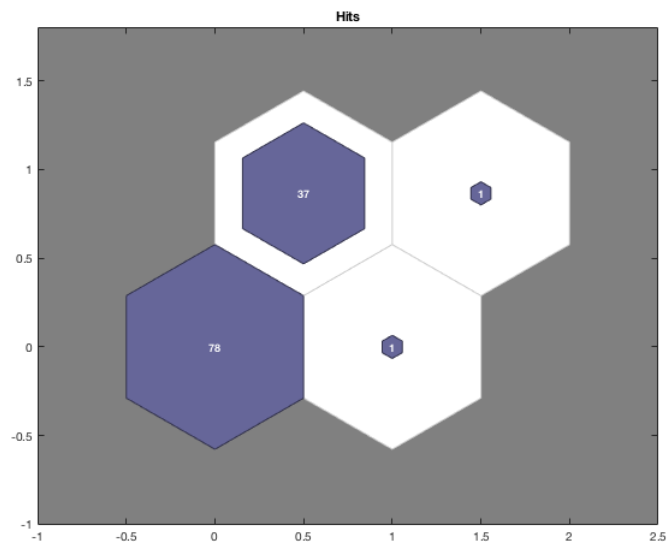


Figure 25: The result of the self-organizing feature map clustering. The number indicates the number of data sets assigned to each cluster.

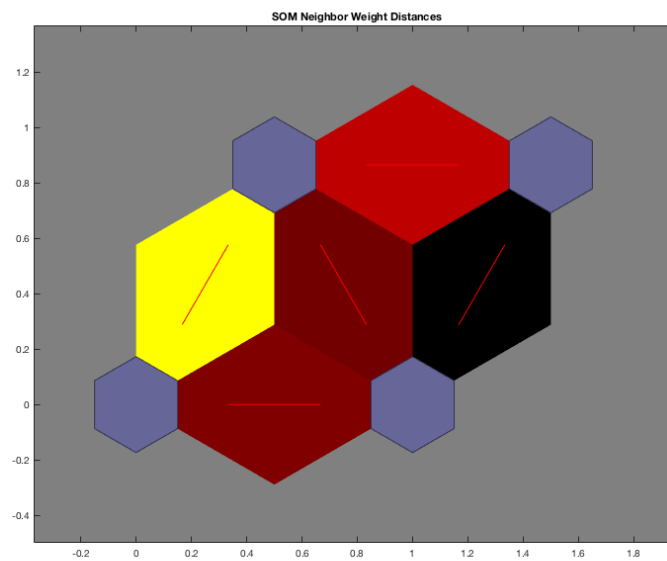


Figure 26: The topological distance between the clusters. The blue blocks are the clusters. A bright colour between clusters indicates small distance, dark colour indicates large distance.



Figure 27: An example of the impact of one of the input parameters on the clustering. A bright colour indicates that the parameter in question (maximum helicity density in the pulmonary artery during early diastole) had a small impact on the cluster, a dark colour indicates a large impact.

5.3 Posterior probabilities

The results from comparing the clustering obtained using the SOFM with the EF labelling can be found in Table 3

Label/cluster belongings	C_1	C_2	C_3	C_4
L_1 (EF < 50%)	40.00%	3.33%	53.33%	3.33%
L_2 (EF \geq 50%)	75.86%	0.00%	24.14%	0.00%

Table 3: The relationship between labels and cluster belongings. Each element (i, j) of the table describes the fraction of the elements labelled as i that were grouped into cluster j , e.g. 40% of the data sets with EF < 50% (L_1) were grouped into cluster 1 (C_1).

The resulting posterior probabilities for the labelling of a data set given its cluster belonging can be seen in Table 4

$P(L_i C_i)$	C_1	C_2	C_3	C_4
L_1 (EF < 50%)	15.38%	100.00%	43.23%	100.00%
L_2 (EF \geq 50%)	84.61%	0.00%	56.77%	0.00%

Table 4: The posterior probabilities. Every element describes the probability of a data set having the label L_i when assigned to the cluster C_j .

6 Discussion

A hemodynamic assessment tool was created to be able to create an automatic hemodynamic overview of a data set. The expected run-time for the analysis of one data set is around 3-4 minutes on a 6-core processor with a speed of 3.5 GHz, and RAM memory of 64 GB. The tool includes calculation of a variety of hemodynamic parameters that have previously shown to be clinically useful. The results are then presented in a way that is easy to interpret.

6.1 The results

6.1.1 Parameter visualisation

Let us start by discussing the plots found in Figs. 14-24. These are the curves corresponding to the parameters evaluated in a number of regions for one single data set (14-18) as well as for an average of the parameters (22) and a single versus the average (24). They all quite clearly depict how their respective parameter behaves over time.

The blood flow speeds seen in Figs. 9 and 10 correspond well to what we know of the behaviour of blood flow through the heart (see Section 2.1.1). The total turbulent kinetic energy in the left ventricle (Fig. 12, top left, Fig. 22, top left) behaves similarly to what has been previously observed for healthy patients [26], both in curve characteristics and order of magnitude. The comparison of average speeds between a patient with aortic stenosis and the average parameter set can be seen in Fig. 23. The speeds behave quite similarly despite the cardiac illness of the patient. However, other parameters behave differently. In Fig. 24 we see a clear increase in total TKE for the patient with aortic stenosis compared to the total TKE of the average healthy volunteers. This coincides well with what has been shown previously [45]. If we look at the middle-left volume render in Fig. 19, this also becomes very evident. During peak systole when the blood leaves the left ventricle and flows into the aorta, the narrowing of the aortic valves associated with aortic valve stenosis causes a clearly visible increase in TKE.

One thing should be noted for all curves related to TKE. In the early time frames a clear spike can be seen in almost all curves, regardless of region. This is due to an artefact from the MRI

acquisition process. Thus, the initial time frames of these curves should be ignored.

When it comes to pressure differences in the left atrium/ventricle and the aorta, the calculations were based on two previous articles. When comparing the results in Figs. 17 and 18 to the results presented in these articles ([38, 40]), they seem to be in accordance to one another.

In Fig. 22 we see the average total TKE for a number of healthy data sets, with the red bars indicating the standard deviation. However, the standard deviation does not take into account the distribution of the data points. For example, if most data points are very close to one another, but one data point deviates greatly from the rest, the manner of deviation reflected by the standard deviation will be affected. A possible improvement that could be made here is to calculate two standard deviations for each time point, one from the data points above the mean, and one from data points below the mean.

However, for many of the parameters and regions it is more difficult to find studies to compare to. For example, the number of studies regarding the right side of the heart is smaller compared to the left side, and thus the tools' results are harder to evaluate.

6.1.2 Data analysis

There are a number of things that can be said with regards to the statistical analysis of the parameters. The posterior probabilities in Table 4 tell us that if a data set ends up in cluster 1, there is a 84% probability that it also has an EF over 50%. While this might seem to be a clear and useful result, there are a few things that need to be mentioned. The first thing is that, as mentioned before (section 2.1.3), different articles and studies define healthy EF differently. This could raise questions about the usefulness of the results. The second and fourth column of table 4 should probably be ignored, as the clusters corresponding to these columns only have one data set in them each. When it comes to the third cluster, we see that the probability of a data set having a certain label when grouped to that cluster is close to a coin flip. Thus, the only piece of possibly useful information comes from the posterior probabilities related to the first cluster.

Could some other label have been used for comparison? While we have some information about the condition of the patients, it is hard to use different diseases to infer a strict labelling. Many of the data sets belong to a group of patients with varying degrees of chronic ischemic heart disease, which means that we did not necessarily expect unsupervised classification to result in a straightforward clustering. To achieve proper, interesting labelling, it would be beneficial to have a (group of) physician(s) sit down and analyse the data sets and come up with a more specific labelling that is not only accurate, but also more likely to be relevant.

Other points of uncertainty can be found by looking at the SOFM clustering. While the used method is applicable for problems such as ours, the question of whether the clustering obtained actually makes sense can still be asked. The SOFM neural network tool used for

the analysis grouped the vast majority of data sets into one of two clusters (Fig. 25), but by looking at the topological distance between the two major clusters, in Fig. 26, we see that the two clusters are actually quite similar. This indicates that the used method for clustering might not be optimal given our data, and that any conclusions drawn based on this clustering should probably be regarded with care. Another factor that one needs to keep in mind is the fact that when applied several times to the same data set, the clustering will vary. The manual selection of the number of clusters is also worth mentioning. A possible way to work around this would be to allow the clustering tool to perform clustering several times, with a varying number of clusters. Then, the desired data set labels could be compared to the different available networks. Any clear and “true” correlation between labels and clusters would then hopefully shine through for a large number of the different networks.

Yet another approach would be to find and implement several other statistical methods of analysis suited for our problem. Potential models of interest could be an adaptive resonance theory-based model, or a model that makes use of Gaussian mixture variational encoders.

The clustering is obviously impacted by the data used, and thus some comments need to be made regarding this. Feature scaling is used to bring all of the parameters into the range $[0, 1]$. This does, however, not eliminate the impact of outlier data points. Any outliers will cause the “real” range of the parameters to be skewed, potentially eliminating the impact of some parameters. A solution to this could be to only use the 95 percentile of the data, however that would risk eliminating potentially interesting information. It also has to be said that the data used in the analysis is fairly heterogeneous. If one was to compare data from only two very distinct patient groups, then the separation into clusters might have been clearer.

It would be interesting to evaluate which parameters have the largest impact when it comes to separating the data into different groups. Such information is provided by the SOFM NN tool that was used, however it was not very easily accessible when a large number of parameters were used for classification. An example of one such piece of information can be seen in Fig. 27. Quantitative information about parameter impact was not available. The information we can extract visually from these plots however, tells us that for this particular clustering, the parameters listed below are some of those that seem to have a relatively large impact on the clustering. In this segment, the following abbreviations are used: s = systole, ed = early diastole, ld = late diastole.

In the left ventricle: average speed (ed) and total TKE (ld).

In the right ventricle: minimum helicity density (ld) and maximum TKE (s).

In the left atrium: average helicity density (ed), maximum helicity density (ed), total KE (ed), average speed (ed), and maximum speed (ed).

In the aorta: average relative helicity (ed + ld), and maximum helicity density (ld).

In the pulmonary artery: maximum helicity density (ed + ld), minimum helicity density (ed), and maximum TKE (ld).

Other parameters that seem to have had an impact were the maximum pressure in the left atrium/ventricle (ed), the pressure difference in the aorta (ed) and the time to peak pressure

in the right atrium/ventricle.

This information should also be regarded with care however. Even though the impact these parameters have on the two major clusters are very different compared to each other, one still has to remember that the two major clusters are topologically quite close to one another. This means that parameters that have a relatively large impact on one of the clusters, but not on the other, might still be similar between data sets in the two clusters.

6.2 The hemodynamic assessment tool

When it comes to the tool itself, there are a number of things that can be said. The tool is innately useful as it provides and makes information accessible - for physicians and researchers alike. Many of the parameters calculated have not been studied extensively in all of the different regions of the heart. One example is the fact that the left side of the heart and the aorta had received more attention from the research community than the right side of the heart. Searching for the keywords “left ventricular” on the web page of the *Journal of the American College of Cardiology* (JACC) yields around 27700 results, while searching for “right ventricular” only yields around 8000. While this is a very rough metric, it can still serve as an indicator for where the focal point of most studies lie. The hemodynamic assessment tool could possibly be a step in another direction, as it provides information about aspects of blood flow behaviour in regions that might not have been widely regarded before. Another advantage of the tool, which also plays into the fact that the need for information about certain aspects of blood flow behaviour may change, is that it can easily be changed or modified to include several more parameters.

Yet another advantage of the tool is the ability to display information about some parameters not only using numbers or curves, but rather in three-dimensional volumes, over time. An example of this in conjunction with a segmentation of the heart is seen in Fig. 19. Displaying the parameters in this way enables easy assimilation of information for the viewer. In this image, only three different time frame per parameters are displayed, but this type of visualisation is also available as a continuous display of all time frames as a movie. These visualisations are useful for visual assessment of the blood flow and parameters related to blood flow.

Before creating the tool, a discussion regarding which parameters to include was held. However, the choice to not include some parameters does not mean that they are of no interest. Possible additions include both the evaluation of parameters already included, but in more regions, and addition of new parameters altogether. One possible parameter extension that could be made is to also include pressure difference calculations in the pulmonary artery. Pressure in the pulmonary artery is a measurement used to define pulmonary arterial hypertension [46], but the measurement used for definition is the mean of absolute pressure. Since the pressure fields we calculate are relative (see Section 3.1.6), these cannot be used for this type of assessment. All the same, this does not exclude that pressure differences between e.g. the pulmonary trunk and points in the right and left main pulmonary arteries could be

of interest. Pressure differences are already used for assessment of stenoses in the aorta and ventricles (see Section 3.1.6), and should therefore also be of interest regarding stenoses in the pulmonary artery.

Another hemodynamic parameter that could possibly be included is wall shear stress (WSS), which has been studied in relation to patients with bicuspid aortic valves (as opposed to the normal tricuspid) [47]. However, actual WSS is often underestimated by MRI [48]. Despite this, the measurements obtained could still be interesting.

One of, if not the most commonly measured hemodynamic parameter is flow volume. Much like blood speed, it can be used to quantify other aspects of blood flow, but blood flow volume can in itself be an interesting parameter. Flow volume could be assessed as the flow volume through one or several planes in the region of interest.

6.3 Future work

Are there any calculations that could have been done differently? One of the main improvements that could be made to the tool is to try and add to the robustness of some of the calculations. Some of the calculations that have to do with different points in time contain elements that were arbitrarily selected by hand. For example, when finding the end of systole, the time frame chosen was simply the location of the aortic speed peak plus an arbitrary number. While the tool functions well despite this, it is something that could probably be done in a more general sense to add to the robustness of the tool. As a small compensation for this, the tool provides the user with information most of the time when a decision is made due to one of these arbitrary conditions.

The two points that are used for pressure difference calculations in the aorta could also be obtained in a better and more robust way. If the segmentation used for the aorta is flawed, the tool can have a hard time identifying where to put the points. This mostly happens in the descending aorta. There are more refined methods for calculating centerlines in vessels, and to improve the tool further, one of these could be implemented. For example, a fast marching and Runge-Kutta based method has been developed with the purpose of finding centerlines in the coronary artery [49].

The pressure difference points in the right ventricle also need to be mentioned. The method used to obtain these points is the same as for the left ventricle. However, the shape of the right ventricle is quite different to the one of the left ventricle. Where the left ventricle is cone-shaped, the right ventricle is crescent-shaped. Since the point calculation method walks in a straight line between atrial and ventricular centroids, it does not take into account the crescent shape of the right ventricle. This means that while the location of the base of the right ventricle might be correct, the location of the “apex” might not. Instead of calculating a point towards the end of the crescent shape, a point closer towards the middle will be chosen. Once the ventricle starts “bending”, the line between the centroids of the atrium and ventricle

will go through the ventricle wall instead of following through towards the end of the ventricle. A possible solution to this could be to, again, use some kind of centerline approximation of the right ventricle. This might be difficult due to the wider shape of the ventricle compared to that of blood vessels, but could still be worth an attempt.

7 Conclusions

In this project, a tool for the automatic assessment of a number of hemodynamic parameters has been created. The tool takes four-dimensional blood flow data as input, and outputs a number of parameters. Through use of the hemodynamic assessment tool, characteristics of blood flow can be easily visualised and analysed. Physicians and researchers alike can use this tool in order to access information about the blood flow through the heart.

The addition of more information and knowledge with regards to cardiac blood flow could possibly be a step towards finding new correlations between blood flow and cardiac disease. Physicians could use this information in the treatment process of patients with heart disease. Furthermore, the tool can help in finding new areas of research interest.

A small statistical analysis of the hemodynamic parameters obtained from applying the tool on a number of data sets with regards to ejection fraction did not yield any significant results. By refining the methods used, and by further investigation with regards to the labelling of the data sets, a statistical analysis that shows correlation between blood flow parameters and different cardiac related labels could possibly be obtained. Information about which hemodynamic parameters provides the most information when it comes to different types of heart disease is something that could be very useful.

In the future, the tool will hopefully be further developed and improved. More parameters could be added, and the calculation of ones that are already present could be refined. The hemodynamic assessment tool has great potential to enable and facilitate the work of doctors, and by extension the treatment and quality of life of patients with cardiac disease.

8 References

- [1] Markl M, Geiger J, Kilner PJ, Foll D, Stiller B, Beyersdorf F, Arnold R, Frydrychowicz A. "Time-resolved three-dimensional magnetic resonance velocity mapping of cardiovascular flow paths in volunteers and patients with Fontan circulation" *Eur J Cardiothorac Surg*. 2011;39:206–212.
- [2] Richter Y, R. Edelman E, "Cardiology Is Flow", *Circulation*, 113:2679-2682, 2006
- [3] Markl M, Kilner P J, and Ebberts T, "Comprehensive 4D velocity mapping of the heart and great vessels by cardiovascular magnetic resonance," *Journal of Cardiovascular Magnetic Resonance*, vol. 13, no. 1, p. 7, 2011.
- [4] Hope M D, Sedlic T, and Dyverfeldt P, "Cardiothoracic magnetic resonance flow imaging", *Journal of thoracic imaging*, vol. 28, no. 4, pp. 217–30, 2013.
- [5] Carlhäll C-J, F. Bolger A, "Passing Strange, Flow in the Failing Ventricle", *Circulation: Heart Failure*, March 2010, Volume 3, Issue 2
- [6] Eriksson J, Dyverfeldt P, Engvall J, F. Bolger A, Ebberts T, and Carlhäll C-J, "Quantification of presystolic blood flow organization and energetics in the human left ventricle", *American Journal of Physiology - Heart and Circulatory Physiology*, Volume 300, Issue 6, June 2011, pp. H2135-H2141
- [7] O. Mangual J, Kraigher-Krainer E, De Luca A, Toncelli L, Shah A, Solomon S, Galanti G, Domenichini F, Pedrizzetti G, "Comparative numerical study on left ventricular fluid dynamics after dilated cardiomyopathy", *Journal of Biomechanics*, June 21, 2013, Volume 46, Issue 10, pp. 1611–1617
- [8] Caro C.G., Pedley T.J., Schroter R.C. and Seed W.A., "The Mechanics of the Circulation", Oxford University Press, 1978
- [9] "Cross section of the heart", viewed 5/4/2018. URL: <https://www.thoughtco.com/ventricles-of-the-heart-373254>
- [10] Kosaraju A, Makaryus AN. "Left Ventricular Ejection Fraction". [Updated 2017 Oct 11]. In: StatPearls [Internet]. Treasure Island (FL): StatPearls Publishing; 2018 Jan-. Available from: <https://www.ncbi.nlm.nih.gov/books/NBK459131/>
- [11] K.K. Poppe, on behalf of The EchoNoRMAL Collaboration; "What is normal left ventricular ejection fraction? a global individual person data meta-analysis of the distribution across ethnicity, gender and age", *European Heart Journal*, Volume 34, Issue suppl.1, 1 August 2013, 1938, <https://doi.org/10.1093/eurheartj/eh308.1938>
- [12] Kawel-Boehm N, Maceira A, R Valsangiacomo-Buechel E, Vogel-Claussen J, B Turkbey E, Williams R, Plein S, Tee M, Eng J, and A Bluemke D, "Normal values for cardiovascular magnetic resonance in adults and children", *Journal of Cardiovascular magnetic resonance*, 2015; 17(1): 29.

-
- [13] Dyverfeldt P, Bissell M, J. Barker A, F. Bolger A, Carlhäll C-J, Ebberts T, J. Francios C, Frydrychowicz A, Geiger J, Giese D, D. Hope M, J. Kilner P, Kozerke S, Myerson S, Neubauer S, Wieben O, Markl M, "4D flow cardiovascular magnetic resonance consensus statement", *Journal of Cardiovascular Magnetic Resonance* (2015) 17:72
- [14] Rohlfing T, Brandt R, Menzel R, Russakoff DB, Maurer CR (2005) "Quo vadis, atlas-based segmentation?", Springer, Boston
- [15] Bustamante M, Petersson S, Eriksson J, Alehagen U, Dyverfeldt P, Carlhäll C-J and Ebberts T, "Atlas-based analysis of 4D flow CMR: Automated vessel segmentation and flow quantification", *Journal of Cardiovascular Magnetic Resonance* 2015 17:87
- [16] Bustamante M, Gupta V, Carlhäll C-J and Ebberts T, "Improving visualization of 4D flow cardiovascular magnetic resonance with four-dimensional angiographic data: generation of a 4D phase-contrast magnetic resonance CardioAngiography (4D PC-MRCA)", *Journal of Cardiovascular Magnetic Resonance* 2017 19:47
- [17] Eriksson J, Bolger AF, Ebberts T, Carlhäll C-J. "Four-dimensional blood flow-specific markers of LV dysfunction in dilated cardiomyopathy". *Eur Heart J-Card Img.* 2013;14(5):417–424.
- [18] Stoll VM, Loudon M, Eriksson J, Bissell MM, Dyverfeldt P, Ebberts T, Myerson SG, Neubauer S, Carlhäll C-J, Hess AT, "Test-retest variability of left ventricular 4D flow cardiovascular magnetic resonance measurements in healthy subjects", *Journal of Cardiovascular Magnetic Resonance*, 2018 Mar 2;20(1):15
- [19] Köhler B, Born S, F. P. van Pelt R, Hennemuth A, Preim U and Preim B, "A Survey of Cardiac 4D PC-MRI Data Processing" *Computer graphics forum* Volume 36 (2017), number 6 pp. 5–35
- [20] Akins C W, Travis B, Yoganathan A P, "Energy loss for evaluating heart valve performance", *The Journal of Thoracic and Cardiovascular Surgery* 136, 4 (2008), 820–833. doi:10.1016/j.jtcvs.2007.12.059.
- [21] Clark C, "Turbulent velocity measurements in a model of aortic stenosis", *Journal of Biomechanics* 9, 11 (1976), 677–687. doi:10.1016/0021-9290(76)90169-X.
- [22] Dyverfeldt P, Escobar Kvitting J-P, Sigfridsson A, Engvall J,F. Bolger A, MD,1,5 and Ebberts T, "Assessment of Fluctuating Velocities in Disturbed Cardiovascular Blood Flow: In Vivo Feasibility of Generalized Phase-Contrast MRI", *Journal of magnetic resonance imaging* 28:655–663 (2008)
- [23] Dyverfeldt P, Sigfridsson A, Escobar Kvitting J-P, and Ebberts T, "Quantification of intravoxel velocity standard deviation and turbulence intensity by generalizing phase-contrast MRI", *Magn. Reson. Med.* 56, 850–858. doi: 10.1002/mrm.21022(2006).
- [24] Ha H, Ziegler M, Welander M, Bjarnegård N, Carlhäll C-J, Lindenberger M, Länne T, Ebberts T and Dyverfeldt P (2018), "Age-Related Vascular Changes Affect Turbulence in Aortic Blood Flow." *Front. Physiol.* 9:36. doi: 10.3389/fphys.2018.00036

-
- [25] Fredriksson A, Trzebiatowska-Krzynska A, Dyverfeldt P, Engvall J, Ebberts T, Carlhäll C-J, "Turbulent kinetic energy in the right ventricle: Potential MR marker for risk stratification of adults with repaired Tetralogy of Fallot", *Journal of magnetic resonance imaging* vol. 47, Pages 1043-1053, Issue 4, April 2018
- [26] Zajac J, Eriksson J, Dyverfeldt P, F. Bolger A, Ebberts T, and Carlhäll C-J, "Turbulent Kinetic Energy in Normal and Myopathic Left Ventricles", *Journal of magnetic resonance imaging* 41:1021–1029 (2015)
- [27] Reiter G, Reiter U, Kovacs G, Kainz B, Schmidt K, Maier R, Olschewski H, Rienmueller R, "Magnetic Resonance–Derived 3-Dimensional Blood Flow Patterns in the Main Pulmonary Artery as a Marker of Pulmonary Hypertension and a Measure of Elevated Mean Pulmonary Arterial Pressure", *Circulation: Cardiovascular Imaging*, 2008;1:23-30, Originally published July 1, 2008
- [28] Schäfer M, J. Barker A, Kheyfets V, R. Stenmark K, Crapo J, E. Yeager M, Truong U, J. Buckner K, E. Fenster B and S. Hunter K, "Helicity and Vorticity of Pulmonary Arterial Flow in Patients With Pulmonary Hypertension: Quantitative Analysis of Flow Formations", *Journal of the American Heart Association* 2017;6:e007010, originally published December 20, 2017
- [29] Gerard M. London, "The concept of ventricular/vascular coupling: functional and structural alterations of the heart and arterial vessels go in parallel", *Nephrol Dial Transplant* (1998) 13: 250–253
- [30] Lorenz R, Bock J, Barker A. J, von Knobelsdorff-Brenkenhoff F, Wallis W, Korvink J. G, Bissell M. M, Schulz-Menger J, Markl M.: "4D Flow magnetic resonance imaging in bicuspid aortic valve disease demonstrates altered distribution of aortic blood flow helicity", *Journal of Magnetic Resonance in Medicine* 71, 4 (2014), 1542–1553. doi:10.1002/mrm.24802.
- [31] <https://www.123sonography.com/diastolic-function-and-diastolic-dysfunction>, 28/03/2018
- [32] <https://www.123sonography.com/book/338>, 28/03/2018
- [33] Eriksson J, F. Bolger A, Carlhäll C-J, and Ebberts T. "Spatial Heterogeneity of Four-Dimensional Relative Pressure Fields in the Human Left Ventricle", *Magnetic Resonance in Medicine* 74:1716–1725 (2015)
- [34] American Heart Association, http://www.heart.org/HEARTORG/Conditions/More/HeartValveProblemsandDisease/Problem-Heart-Valve-Stenosis_UCM_450369_Article.jsp, 4/04/2018
- [35] Courtois, M, Kovacs, S. J. and Ludbrook, P. a. (1990). "Physiological early diastolic intraventricular pressure gradient is lost during acute myocardial ischemia", *Circulation* 81(5): 1688–1696.

-
- [36] Ebbers T, Wigström L, Bolger A. F, Engvall J, and Karlsson M (2001), "Estimation of relative cardiovascular pressures using time-resolved three-dimensional phase contrast MRI", *Magnetic Resonance in Medicine* 45(5): 872–879.
- [37] Panton R. (1984). "Incompressible Flow", John Wiley & Sons Australia, Limited.
- [38] Kuş E, "Estimation and visualization of relative pressure fields in the human heart from time resolved MRI flow data", Linköping University, 2013
- [39] Ebbers T, Wigström L, Bolger AF, Wranne B, Karlsson M, "Noninvasive measurement of time-varying three-dimensional relative pressure fields within the human heart". *Journal of Biomechanical Engineering* 2002;124:288–293.
- [40] Ebbers T, Farnebäck G, "Improving Computation of Cardiovascular Relative Pressure Fields From Velocity MRI", *Journal of Magnetic Resonance Imaging* 30:54–61 (2009)
- [41] Kohonen T, and Honkela T, (2007) "Kohonen network", Scholarpedia, 2(1):1568, revision #122029.
- [42] Kerschnitzki, Kollmannsberger et al., "Architecture of the osteocyte network correlates with bone material quality." *Journal of Bone and Mineral Research*, 28(8):1837-1845, 2013.
- [43] Xiang Q.S., "Temporal phase unwrapping for CINE velocity imaging", *Journal of magnetic resonance imaging: JMRI* 5, 529-34, 1995
- [44] Ebbers T, Haraldsson H, Dyverfeldt P, "Higher order weighted least-squares phase offset correction for improved accuracy in phase-contrast MRI". "Proceedings of the International Society of Magnetic Resonance in Medicine", 16 39 1367
- [45] Dyverfeldt P, D. Hope M, E. Tseng E, and Saloner D, "Magnetic Resonance Measurement of Turbulent Kinetic Energy for the Estimation of Irreversible Pressure Loss in Aortic Stenosis", *JACC Cardiovasc Imaging*, 2013 Jan; 6(1): 64–71.
- [46] J Barst R, McGoon M, Torbicki A, Sitbon O, J Krowka M, Olschewski H, Gaine S, "Diagnosis and differential assessment of pulmonary arterial hypertension", *Journal of the American College of Cardiology* Volume 43, Issue 12, Supplement, 16 June 2004, Pages S40-S47
- [47] D. Hope M, Sigovan M, Wrenn S. J, Saloner S, and Dyverfeldt P, "Magnetic Resonance Imaging Hemodynamic Markers of Progressive Bicuspid Aortic Valve Related Aortic Disease", *Journal of Magnetic Resonance Imaging*, 2014 Jul; 40(1): 140–145.
- [48] D. Hope M, Sedlic T, and Dyverfeldt P, "Cardiothoracic Magnetic Resonance Flow Imaging", *Journal of Thoracic Imaging* Volume 28, Number 4, July 2013
- [49] Cui H, Wang D, Wan M, Zhang J-M, Zhao X, San Tan R, Huang W, Xiong W, Duan Y, Zhou J, Luo T, S. Kassab G, and Zhong L, "Fast Marching and Runge–Kutta Based

Method for Centreline Extraction of Right Coronary Artery in Human Patients”, *Cardiovascular Engineering and Technology*, Vol.7, No.2, June 2016 (2016) pp. 159–169

Master's Theses in Mathematical Sciences 2018:E34
ISSN 1404-6342
LUTFMA-3352-2018
Mathematics
Centre for Mathematical Sciences
Lund University
Box 118, SE-221 00 Lund, Sweden
<http://www.maths.lth.se/>